Astronomy & Astrophysics manuscript no. vascov1.1
January 9, 2009
© ESO 2009

Chemical abundances of 451 stars from the HARPS GTO planet search program ⋆

Thin disk, thick disk, and planets

V. Neves[1,2], N. C. Santos[1,3], S. G. Sousa[1,4], A. C. M. Correia[2], and G. Israelian[5]

[1] Centro de Astrofísica, Universidade do Porto, Rua das Estrelas, 4150-762 Porto, Portugal
[2] Departamento de Física, Universidade de Aveiro, Campus de Santiago 3810-193 Aveiro, Portugal
[3] Observatoire de Genève, 51 ch. des Maillettes, 1290 Sauverny, Switzerland
[4] Departamento de Matemática Aplicada, Faculdade de Ciências da Universidade do Porto, Portugal
[5] Instituto de Astrofísica de Canarias, 38200 La Laguna, Tenerife, Spain

Received XXX; accepted XXX

ABSTRACT

In this paper we present an uniform study of the chemical abundances of 12 elements (Si, Ca, Sc, Ti, V, Cr, Mn, Co, Ni, Na, Mg, and Al) derived from the spectra of 451 stars from one of the HARPS GTO planet search programs. **Sixty eight** of these are planet bearing stars. The main goals of our work are: i) the investigation of the possible differences between the abundances of the stars with and without planets; ii) the study of the possible differences between the abundances of stars from the thin and the thick disk. We confirm that there is an overabundance of metallicity in planet host stars, common to all studied species. We also found that there is no difference in the galactic chemical evolution trends of the stars with and without planets. Stars that harbour planetary companions simply seem to be in the high metallicity tail of the distribution. We also confirm the hints that neptunian and super-earth class planets may be easier to find at lower metallicities. A statistically significative abundance difference between stars of the thin and the thick disk was found for [Fe/H] < 0. However, the populations from the thick and the thin disk are not clearly separated.

Key words. stars: abundances – stars: chemically peculiar – stars: fundamental parameters – stars: planetary systems – galaxy: disk – galaxy: kinematics and dynamics – galaxy: solar neighbourhood

1. Introduction

The discovery that giant planet host stars have, on average, a higher metallicity than non planet hosts (Gonzalez 1997), sparked a flurry of spectroscopic studies using the samples of radial velocity planet hunting programs (e.g. Santos et al. 2001, 2004; Laws et al. 2003; Fischer & Valenti 2005). Gradually, similar abundance studies were made for elements other than iron (e.g. Gonzalez et al. 2001; Sadakane et al. 2002; Israelian et al. 2003; Bodaghee et al. 2003; Beirão et al. 2005; Fischer & Valenti 2005; Gilli et al. 2006; Ecuvillon et al. 2006; Takeda 2007). The same abundance difference was observed in these elements, suggesting that the probability of finding a giant planet is strongly related to the abundance content of its host star.

Interestingly, stars with neptune and super-earth class planets might have different trends than the ones found for jovians. There are hints that such planets may be easier to find at the typical metallicities of non planet (non-jovian?) host stars or even at lower [Fe/H] values (Udry et al. 2006; Sousa et al. 2008). However, there are not enough planets yet to make a sound statistical distribution.

Some authors also referred the existence of different [X/Fe] trends in planet host stars when compared to stars without planets for the same [Fe/H]. These potential differences were detected for some elements (e.g. Si, Ti, Mn, V, Co, Ni, Na, Mg) (e.g. Bodaghee et al. 2003; Gilli et al. 2006; Robinson et al. 2006) and are very difficult to explain by galactic chemical evolution models. Despite that, the obtained results are still contradictory and no definitive conclusion has yet been reached. A review concerning these trends was recently published by Gonzalez & Laws (2007).

The large samples of spectra used in planet search surveys with radial velocity methods may also be employed to study the abundances and kinematic properties of the stars of the solar neighbourhood (e.g. Santos et al. 2003;

⋆ Based on observations collected at the La Silla Parana Observatory, ESO (Chile) with the HARPS spectrograph at the 3.6m telescope, under the GTO program 072.C-0488.

Fischer & Valenti 2005; Gilli et al. 2006; Ecuvillon et al. 2007). This data can be used to study the properties of the different populations of our galaxy and, in particular, the differences between the thin and the thick disk. Fuhrmann et al. (1998) showed that the thick disk stars have a clear [Mg/Fe] overabundance when compared to the stars of the thin disk, for the same [Fe/H], at least for metallicities below solar. This fact was confirmed by Bensby et al. (2003) and expanded for other elements. The work of Ecuvillon et al. (2007), however, did not show any clear difference in the abundances of the elements of the different populations as observed in previous studies.

In this paper, we derive the abundances of twelve species (silica, calcium, titanium, scandium, manganese, chromium, vanadium, cobalt, nickel, sodium, magnesium, and aluminium), based on the spectra of a subsample of one of the HARPS "high precision" guaranteed time observations (GTO) planet search program. This sample contains 451 stars, out of which **68** are planet hosts and the remaining **383** stars are dwarfs with no known orbiting planets (Sousa et al. 2008). We also derive the kinematic properties of the sample. The main goals of this work are twofold: i) the investigation of the possible differences between the abundances of the stars with and without planets; ii) the study of the possible differences between the abundances of stars from the thin and the thick disk of our galaxy. In section 2, we present the sample used in this work, along with the calculation of the galactic space velocity data and the selection of the populations of the different groups of stars, based on their kinematic properties. The method and the selection steps that precede the chemical abundance determination will be explained in section 3. Section 4 contains the abundance analysis of the full sample as well as the final [X/H] values. It also includes the discussion on the uncertainties and errors of our methodology as well as a comparison of our results with the literature. The discussion of the results follows in section 5, where we explore the possible differences between stars with and without planets in our sample. In section 6, we discuss the differences between the abundances of the thin and the thick disk stars, using the [X/Fe] distributions for [Fe/H] < 0 and the [X/Fe] vs [Fe/H] plots. We also use these latter plots to make a brief study on the trends of the galactical chemical evolution. Lastly, on section 7, we make our final concluding remarks.

2. The sample

The spectra for the HARPS "high precision" GTO program were obtained with the HARPS spectrograph at the ESO 3.6m telescope (La Silla, Chile). This sub sample is composed of 451 stars, selected from the volume limited sample of solar neighbourhood stars studied with the CORALIE spectrograph (Udry et al. 2000) as well as a group of planet hosts from the southern hemisphere. Details about this sample are given in Sousa et al. (2008). We need to note that we have updated the original GTO catalogue, using the data from the extrasolar planets encyclopaedia[1], to take into account the newly discovered planets orbiting the stars HD40307 (Mayor et al. 2008), HD47186, and HD181433 (Bouchy et al. in prep.). The total number of planet bearing stars in the sample is now **68**. Most stars in the catalogue are slow rotators, non evolved, and with a low chromospheric activity level.

The individual spectra were reduced using the HARPS pipeline and later combined with IRAF[2] after correcting for their radial velocity. The final spectra have a resolution of $R \sim 110.000$ and a signal to noise ratio ranging from ~ 70 to ~ 2000 depending on the amount and quality of the original spectra. Nine tenths of the spectra have S/N higher than 200 and 50% have a S/N greater than 450.

A solar spectrum was also collected with HARPS using solar light reflected by the asteroid Ceres. This spectrum has the same resolution of the remaining spectra and a S/N ratio of ~ 250.

The stellar parameters used in this paper were determined by Sousa et al. (2008).We refer to this paper for details.

2.1. The UVW Data and Thin/Thick disk stars

The galactic space velocity components (UVW), analysed in section 6, were computed with the trigonometric parallaxes and proper motions from the Hipparcos catalogue (ESA 1997) and making use of the mean radial velocities obtained from the HARPS spectra (courtesy of the HARPS GTO team). The galactic space velocity components were calculated using the procedure from Johnson & Soderblom (1987) and corrected for the solar motion relative to the local standard of rest (LSR) using $(U_\odot, V_\odot, W_\odot) = (+10.00, +5.25, +7.17)$ km s^{-1} from Dehnen & Binney (1998). This LSR correction was also used by Bensby et al. (2003, 2005).

The selection of the thin and thick disk stars was made using the method proposed by Bensby et al. (2003, 2005). The characteristic velocity dispersions $(\sigma_U, \sigma_V, \sigma_W)$, the asymmetric drift, V_{asym}, and the observed fractions of these populations in the solar neighbourhood were taken from Bensby et al. (2005), as well as the equations to calculate the relative probability of a star belonging to a certain population. Each probability (P) is calculated by multiplying its gaussian probability distribution with the observed fraction of the respective population. Following the recommendations of Bensby et al. (2005), if $P_{thickdisk}/P_{thindisk} \geq 2$, the star will be considered a member of the thick disk. Otherwise, if $P_{thickdisk}/P_{thindisk} \leq 0.6$, the star will belong to the thin disk. All remaining stars having a probability between these values will be included in a transition population.

[1] http://exoplanet.eu/

[2] IRAF is distributed by National Optical Astronomy Observatories, operated by the Association of Universities for Research in Astronomy, Inc., under contract with the National Science Foundation, U.S.A.

Table 1. Sample table of the parameters used to calculate the population of each star. Columns 2, 3, and 4 list the U,V and W velocities relative to the local standard of rest (LSR). Columns 5, 6, and 7 list the Gaussian distributions of each population: thin disk, thick disk, and halo, respectively. In columns 8 and 9 we have the relative probabilities of the thick disk relative to the thin disk and of the thick disk relative to the halo. The last column depicts the probable population where each star belongs.

Star ID	U_{LSR}	V_{LSR} [km s^{-1}]	W_{LSR}	f_{thin}	f_{thick}	f_{halo}	$\frac{P(thickdisk)}{P(thindisk)}$	$\frac{P(thickdisk)}{P(halo)}$	group
...	...	...	...	...	...	...	...	...	...
HD134060	26	-34	15	1.75E-06	5.75E-07	5.67E-09	0.02	4059.26	thin
HD134606	-11	-16	1	5.36E-06	5.20E-07	3.80E-09	0.01	5480.99	thin
HD134664	27	2	-14	1.92E-06	2.69E-07	2.26E-09	0.01	4760.19	thin
HD134985	-29	-65	-41	7.14E-09	2.92E-07	9.84E-09	2.61	1187.61	thick
HD134987	-11	-35	28	7.24E-07	4.91E-07	5.62E-09	0.04	3494.89	thin
HD136352	-109	-42	43	4.76E-10	8.89E-08	4.93E-09	11.94	721.81	thick
HD136713	9	-13	-5	5.15E-06	4.84E-07	3.51E-09	0.01	5509.52	thin
HD136894	5	3	0	3.76E-06	3.11E-07	2.28E-09	0.01	5447.19	thin
...	...	...	...	...	...	...	...	...	...

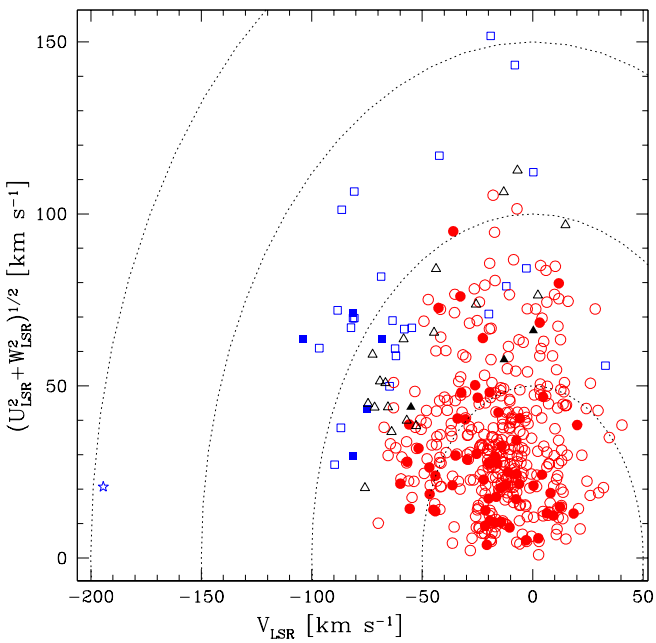

Fig. 1. Toomre diagram for the full sample (451 stars). The stars from the thin disk, transition group, and the thick disk are marked by red circles, black triangles, and blue squares, respectively. The stars with and without planets are shown with full and empty symbols, respectively.The halo star HD104006 is represented by a starred symbol.

The star HD104006, with a $P_{thickdisk}/P_{halo} = 0.286$ will be considered as belonging to the halo.

In Fig. 1, the Toomre Diagram shown represents the whole sample. The blue squares, black triangles and red circles correspond to the thick disk, transition and thin disk stars, respectively. The stars with and without planets are shown with full and empty symbols, respectively. The halo star HD104006 is represented by a starred symbol. A sample of the distributions and the probabilities calculated for each star, as well as the parameters that were used for their calculation, are presented in Table 1.

Among the 451 stars in our sample, we have 400 stars from the thin disk, 29 from the thick disk, and 21 are considered transition stars that don't belong to any group or have a determined origin. According to the used criteria, only 1 star is from the halo.

3. Chemical abundances

The chemical abundances of the studied elements were derived using a differential local thermodynamic equilibrium (LTE) analysis. This was done with the 2002 version of the MOOG[3] program (Sneden 1973) using the "abfind" driver. A grid of Kurucz (1993) ATLAS9 atmospheres, were used as input, along with the equivalent widths and the atomic parameters, wavelength (λ), excitation energy of the lower energy level (χ_l) and oscillator strength ($\log gf$) of each line. The atmospheric parameters, effective temperature (T_{eff}), surface gravity ($\log g$), microturbulence (ξ_t), and metallicity ([Fe/H]) were taken from Sousa et al. (2008) and derived from the same spectra used in our study. This gives consistency to our work, making it more uniform and less subjected to external errors. The reference abundances used in the differential analysis are the ones for the Sun, and were taken from Anders & Grevesse (1989).

3.1. The line-list

The initial line list, along with the atomic parameters (including an initial estimate of the oscillator strengths) were taken from the VALD[4] online database (Piskunov et al. 1995, Kupka et al. 1999). When extracting the lines, we used the Solar stellar parameters as input : $T_{eff} = 5777$ K; $\log g = 4.44$ dex; $\xi_t = 1.0$ km/s. We have found 2169 lines in the spectral region of interest (4500 to 6910 Å). After a lengthy process of selection and identification of

[3] The source code of MOOG2002 can be downloaded at http://verdi.as.utexas.edu/moog.html

[4] Vienna Atomic Line Database

the "good lines", that involved the use of the IRAF 'splot' tool with the Kurucz Solar Flux Atlas (Kurucz et al. 1984), we ended up with a shorter list of 364 lines. All strongly blended lines, as well as lines that were too weak (having Equivalent Widths (hereafter EW) below 5mÅ) , or too strong (lines with EW > 200 mÅ), and those inside the wings of strong lines (e.g. H_α (λ = 6562.81 Å), H_β (λ = 4861.34 Å), λ5172.70, λ5183.62 Mg I lines) were excluded in this process.

The next step involved the automatic measurement of the equivalent width of the lines, in a resolution degraded spectrum ($R \sim$110.000) of the Kurucz Solar Flux Atlas. This was done with the ARES[5] program (Sousa et al. 2007). Here, we have also made a selection procedure that involved the comparison of the EWs measured in the aforementioned spectrum with the one measured in the solar reflected light spectrum of the Ceres asteroid, obtained with HARPS. Both spectra have a resolution of the order of $\sim$ 110.000. If the relative difference between the EWs, for a certain line, measured in the two spectra, was greater than 10%, the line would be discarded. Additionally, we have also excluded all lines that ARES couldn't fit well due to a bad evaluation of the lines in the spectral area of interest, or due to a bad determination of the continuum placement. These criteria are very important because the abundance and especially the oscillator strength determination are very sensitive to variations in the EW. The settings used in ARES were: smoother = 4, space = 2, lineresol = 0.07, miniline = 5 and rejt = 0.996 (from Sousa et al. 2008). At the end of this step, we finished with 284 lines.

The EW of these lines, along with a model atmosphere based on the Solar parameters, $T_{eff} = 5777$, $\log g = 4.44$, $\log \epsilon_{Fe} = 7.47$ and $\xi_t = 1.0$, were used in the calculation of the semi empirical oscillator strengths via an inverse analysis with the MOOG driver 'ewfind'. All input parameters for this driver were taken following Santos et al. (2004). The new oscillator values are very important because the $\log gf$ data from VALD might not be accurate enough.

In order to test the calculated $\log gf$ values, we inverted the previous analysis using a Solar atmosphere model and the measured EWs of the Solar reflected light spectrum of Ceres using the 'abfind' driver within MOOG. In general, the average abundance values found are within 0.01 dex of the expected value except for Al ($\Delta A = \pm 0.04$ with 2 lines), ScI ($\Delta A = \pm 0.03$ with 3 lines) and V ($\Delta A = \pm 0.02$ with 14 lines), where A is the abundance of a species.

The final selection was the most important one. After determining the abundances for all stars, using the Kurucz (1993) model atmospheres, calculated with the stellar parameters and the EWs measured with ARES for each star and element, we divided the stars in three distinct groups: a) the cool group, containing 152 stars with $T_{eff} \leq 5300$; b) the solar group, having 257 stars with $5300 < T_{eff} < 6000$; c) the hot group, comprising 42 stars with $T_{eff} \geq 6000$. This was done to take into account the differences in the local environments around each line that are temperature dependent (Sousa et al. 2008). The ARES parameters were the same as in the Solar case except 'rejt' that changed with the S/N ratio of each spectra, according to Sousa et al. (2008) and 'miniline=2' (making sure that all lines measured in the Solar spectrum were accounted for in the other stars). Then, we calculated the difference between the mean abundance of each line (from all the stars) and the mean abundance calculated using all the lines. This was done for each element, as we can see for Si, shown in Fig. 2 as an example. The open circles in the top, middle and bottom panels, from the hot, solar and cool group stars, respectively, correspond to this difference. The mean value of each line is depicted by a black cross and the error bars represent its rms.

We considered that all the lines showing an overall line dispersion for any plot greater than 1.5 times the rms are

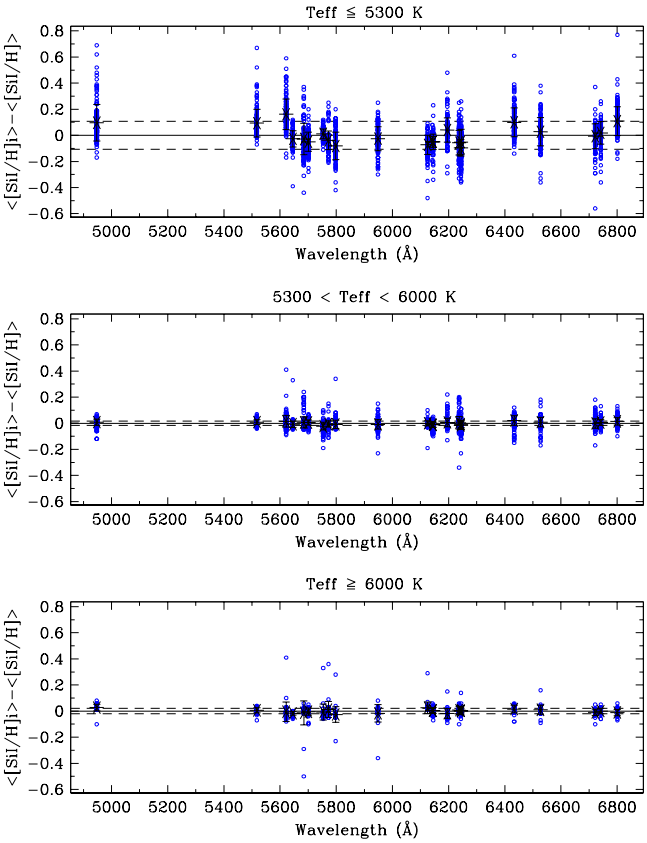

Fig. 2. Process of selection of the stable lines for the neutral atom of Si, shown as example. The black crosses on the three plots are the difference between the mean abundance of each line (from all the stars) and the mean abundance of the element. The error bars represent the rms of the mean values. The dashed lines mark the exclusion value. The open circles correspond to the difference values of the cool group ($T_{eff} \leq$ 5300 - top plot), the solar group (5300 $< T_{eff} <$ 6000 - middle plot) and the hot group ($T_{eff} \geq$ 6000 - bottom plot).

[5] Automatic Routine for Line Equivalent Widths. Available at: http://www.astro.up.pt/ sousasag/ares/

Table 2. Wavelength (λ), excitation potential (χ_l), oscillator strength ($\log gf$) and solar equivalent widths ($EW_\odot$) for the lines selected in the present paper.

λ [Å]	χ_l [eV]	$\log gf$	$EW_\odot$ [mÅ]
Na I - 2 lines, $\log \epsilon_\circ = 6.33$			
5688.22	2.10	-0.628	121.4
6154.23	2.10	-1.622	36.6
6160.75	2.10	-1.363	54.3
Mg I - 3 lines, $\log \epsilon_\circ = 7.58$			
4730.04	4.35	-2.234	69.6
5711.09	4.35	-1.777	105.6
6319.24	5.11	-2.300	25.2
Al I - 2 lines, $\log \epsilon_\circ = 6.47$			
6696.03	3.14	-1.571	36.2
6698.67	3.14	-1.886	21.1
Si I - 18 lines, $\log \epsilon_\circ = 7.55$			
5517.54	5.08	-2.496	12.9
5645.61	4.93	-2.068	35.8
5684.49	4.95	-1.642	61.2
5701.11	4.93	-2.034	37.7
5753.64	5.62	-1.333	45.7
5772.15	5.08	-1.669	52.0
5797.87	4.95	-1.912	43.9
5948.54	5.08	-1.208	85.4
6125.02	5.61	-1.555	31.7
6142.49	5.62	-1.520	33.1
6145.02	5.62	-1.425	38.8
6195.46	5.87	-1.666	17.1
6237.33	5.61	-1.116	61.1
6243.82	5.62	-1.331	44.8
6244.48	5.62	-1.310	46.2
6527.21	5.87	-1.227	38.9
6721.85	5.86	-1.156	44.0
6741.63	5.98	-1.625	15.5
Ca I - 12 lines, $\log \epsilon_\circ = 6.36$			
5261.71	2.52	-0.677	97.7
5349.47	2.71	-0.581	94.6
5512.98	2.93	-0.559	84.8
5867.56	2.93	-1.592	25.1
6156.02	2.52	-2.497	9.6
6161.29	2.52	-1.313	60.6
6166.44	2.52	-1.155	69.9
6169.04	2.52	-0.800	92.2
6449.82	2.52	-0.733	98.1
6455.60	2.52	-1.404	56.3
6471.67	2.53	-0.825	91.2
6499.65	2.52	-0.917	85.8
Sc I - 3 lines, $\log \epsilon_\circ = 3.10$			
4743.82	1.45	0.297	8.0
5520.50	1.87	0.562	6.6
5671.82	1.45	0.533	14.6
Sc II - 6 lines, $\log \epsilon_\circ = 3.10$			
5526.82	1.77	0.140	76.3
5657.88	1.51	-0.326	66.9
5667.14	1.50	-1.025	33.9
5684.19	1.51	-0.946	37.2
6245.62	1.51	-1.022	34.9
6320.84	1.50	-1.863	8.1
Ti I - 30 lines, $\log \epsilon_\circ = 4.99$			
4555.49	0.85	-0.575	63.7
4562.63	0.02	-2.718	10.9
4645.19	1.73	-0.666	22.0
4656.47	0.00	-1.308	68.6
4675.11	1.07	-0.939	38.1
4722.61	1.05	-1.433	18.7
4820.41	1.50	-0.429	43.1
4913.62	1.87	0.068	50.2
4997.10	0.00	-2.174	31.6
5016.17	0.85	-0.657	63.2
5039.96	0.02	-1.199	75.3
5064.06	2.69	-0.471	5.5
5071.49	1.46	-0.797	28.8
5113.44	1.44	-0.861	27.0
5145.47	1.46	-0.622	37.0
5219.70	0.02	-2.254	28.1
5490.16	1.46	-1.008	21.4
5503.90	2.58	-0.218	12.3
5648.57	2.49	-0.410	10.1
5662.16	2.32	-0.123	23.5
5739.48	2.25	-0.781	7.7
5766.33	3.29	0.326	9.6
5965.84	1.88	-0.492	26.7
5978.55	1.87	-0.602	22.6
6064.63	1.05	-1.941	8.3
6091.18	2.27	-0.445	15.0
6126.22	1.07	-1.416	22.1
6258.11	1.44	-0.435	51.5
6261.10	1.43	-0.491	49.2
6599.12	0.90	-2.069	9.3
Ti II - 8 lines, $\log \epsilon_\circ = 4.99$			
4583.41	1.16	-2.840	31.8
4636.33	1.16	-3.152	19.8
4657.20	1.24	-2.379	49.3
4708.67	1.24	-2.392	48.9
4911.20	3.12	-0.537	52.3
5211.54	2.59	-1.490	32.8
5381.03	1.57	-1.904	59.1
5418.77	1.58	-2.104	49.5
Mn I - 6 lines, $\log \epsilon_\circ = 5.39$			
4502.21	2.92	-0.523	57.0
4671.77	2.89	-1.567	14.8
4739.11	2.94	-0.462	60.1
5377.62	3.84	-0.068	40.8
5399.47	3.85	-0.104	38.5
5413.67	3.86	-0.476	21.6
Cr I - 22 lines, $\log \epsilon_\circ = 5.67$			
4575.11	3.37	-1.004	10.0
4600.75	1.00	-1.457	82.3
4626.18	0.97	-1.467	83.3
4633.25	3.13	-1.215	10.4
4700.61	2.71	-1.464	14.0
4708.02	3.17	-0.104	55.0
4730.72	3.08	-0.345	46.3
4767.86	3.56	-0.599	16.1
4775.14	3.55	-1.025	6.9
4936.34	3.11	-0.343	45.6
4964.93	0.94	-2.577	38.1
5214.14	3.37	-0.784	16.4
5238.97	2.71	-1.427	15.9
5247.57	0.96	-1.618	82.0
5287.18	3.44	-0.954	10.4
5296.70	0.98	-1.373	93.1
5300.75	0.98	-2.125	58.9
5781.18	3.32	-0.886	15.5
5783.07	3.32	-0.472	31.4
5787.92	3.32	-0.183	46.0
6661.08	4.19	-0.234	12.0
6882.52	3.44	-0.392	32.2
Cr II - 3 lines, $\log \epsilon_\circ = 5.67$			
4588.20	4.07	-0.752	68.5
4592.05	4.07	-1.252	47.6
4884.61	3.86	-2.069	23.4
V I - 7 lines, $\log \epsilon_\circ = 4.00$			
5670.85	1.08	-0.482	18.8
5737.07	1.06	-0.815	10.4
6081.45	1.05	-0.692	14.1
6224.51	0.29	-1.935	5.3
6251.83	0.29	-1.431	15.0
6274.66	0.27	-1.751	8.3
6285.17	0.28	-1.676	9.5
Co I - 9 lines, $\log \epsilon_\circ = 4.92$			
4594.63	3.63	-0.279	12.5
4792.86	3.25	-0.080	32.7
4813.48	3.22	0.177	45.9
5301.05	1.71	-1.950	19.5
5342.71	4.02	0.606	32.3
5352.05	3.58	0.004	24.4
5359.20	4.15	0.040	9.6
5647.24	2.28	-1.594	14.0
6814.95	1.96	-1.822	18.8
Ni I - 48 lines, $\log \epsilon_\circ = 6.25$			
4512.99	3.71	-1.467	19.4
4811.99	3.66	-1.363	25.6
4814.60	3.60	-1.670	16.7
4913.98	3.74	-0.661	55.7
4946.04	3.80	-1.224	26.2
4952.29	3.61	-1.261	32.3
4976.33	1.68	-3.002	37.7
4995.66	3.63	-1.611	17.9
5010.94	3.63	-0.901	48.8
5081.11	3.85	0.064	93.5
5094.41	3.83	-1.108	30.3
5392.33	4.15	-1.354	12.0
5435.86	1.99	-2.432	51.7
5462.50	3.85	-0.880	41.0
5587.87	1.93	-2.479	52.9
5589.36	3.90	-1.148	26.7
5625.32	4.09	-0.731	37.8
5628.35	4.09	-1.316	14.7
5638.75	3.90	-1.699	9.8
5641.88	4.11	-1.017	24.1
5643.08	4.16	-1.234	15.1
5694.99	4.09	-0.629	43.1
5748.36	1.68	-3.279	28.0
5805.22	4.17	-0.604	40.8
5847.00	1.68	-3.410	23.0
5996.73	4.24	-1.010	20.3
6086.29	4.27	-0.471	43.5
6108.12	1.68	-2.512	65.0
6111.08	4.09	-0.823	34.2
6119.76	4.27	-1.316	10.9
6128.98	1.68	-3.368	25.3
6130.14	4.27	-0.938	22.1
6175.37	4.09	-0.534	49.0
6176.82	4.09	-0.266	63.7
6177.25	1.83	-3.538	14.6
6186.72	4.11	-0.888	30.5
6204.61	4.09	-1.112	22.0
6223.99	4.11	-0.954	27.7
6230.10	4.11	-1.132	20.6
6322.17	4.15	-1.164	18.4
6327.60	1.68	-3.086	38.6
6360.81	4.17	-1.145	18.5
6378.26	4.15	-0.830	31.8
6598.60	4.24	-0.914	24.9
6635.13	4.42	-0.779	23.6
6767.78	1.83	-2.136	79.2
6772.32	3.66	-0.963	49.2
6842.04	3.66	-1.496	24.2

considered non stable lines and are excluded. The dashed lines on the plots of Fig. 2 mark this exclusion value. We also excluded any line with a dispersion on any plot clearly out of the average abundance value. This selection was done with a careful manual inspection line by line and element by element. In a few cases we chose to relax the rules a little, especially when we had a line very close to the exclusion values occurring in only one group. We also verified each line for stray points clearly out of the 2σ distribution (due to bad pixels, cosmic rays or other unknown effects) that could modify the true value of the mean or the dispersion of a certain line and lead to a wrong exclusion. After this last selection, the final list ended up with 180 lines, as shown in Table 2.

4. Abundance analysis of the full sample

As we stated before, the chemical abundances of the elements were derived using a differential LTE analysis relative to the Sun. The analysis of the full 451 star sample was already described in subsection 3.1. The final abundance for each star and element are just the average value of the abundances of every line in a given star and for a given element. A set of FORTRAN programs were made to coordinate the calculations and set up an organised and easy to use database for the output data. A sample of our results are presented in Table 3. The complete results are available online.

4.1. Uncertainties and errors

Uncertainties can introduce different errors in the calculated abundances. Random errors can affect individual lines in the measurement of EWs (e.g. due to noise and cosmic rays) and systematic errors can surface, for example, due to blending, NLTE effects or to a poor location of the continuum. To minimise both types of errors, we should have high quality data and as many lines as possible for each element. Unfortunately, we were only able to select 2 or 3 lines for Na, Mg, Al, ScI and CrII. The lack of statistical data provokes higher internal random errors and it also might introduce systematic bias extremely difficult to locate in our results. Therefore, all conclusions regarding these elements should be taken with caution. We further note that we performed an uniform analysis of the sample. This minimises possible errors due to differences in line lists, atmospheric parameters, oscillator strength biases, applied methodologies, etc.

4.1.1. Random errors

The typical rms uncertainties for the atmospheric parameters are 24 K for T_{eff}, 0.04 dex for $\log g$, 0.02 dex for [Fe/H] and 0.03 km s^{-1} for ξ_t. **These uncertainties come from Sousa et al. (2008) and characterize the precision of the derived parameters.**

We tested the sensitivity of the derived abundances for the uncertainties in the atmospheric parameters. First, for each parameter, we chose three different stars having similar atmospheric parameters except for the one being tested. Afterwards, we generated new atmospheric models, changing the tested parameter by an adequated value in order to assure that the sensitivity of the abundances could be clearly observed (ΔT_{eff} = ±100 K, $\Delta \log g$ = ±0.3 dex, $\Delta\xi_t$ = ±0.5 km s^{-1} and Δ[Fe/H] = ±0.3 dex). The obtained results are displayed in Table 4.

In general, we can observe that the neutral elements are very sensitive to temperature changes, whereas the ions are most sensitive to changes in surface gravity. The ions are also more sensitive to metallicity changes than the neutral elements, although the sensitivity is not as great as the one in T_{eff} and $\log g$.

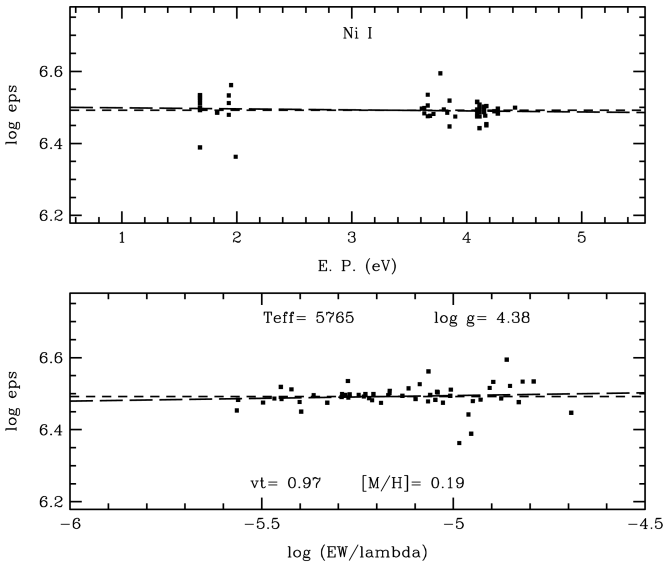

Fig. 3. Example of the calculation of the EP and RW slopes for NiI lines for the star HD1461. The squares represent the different spectral lines, the long dashed line the calculated slope and the short dashed line the average value of the abundance (log eps). The values of the slopes are -0.010 and 0.020, respectively for the upper and lower panel.

4.1.2. Testing the stellar parameters

In order to verify the validity of the stellar parameters, we tested our results in a variety of ways. First, we calculated the slopes of the derived abundances of the considered lines as a function of the excitation potential (EP) and as a function of the logarithm of the reduced equivalent width (RW) for the NiI lines. In this way we can verify if the excitation equilibrium that was forced for the FeI lines on every star and used to obtain the stellar parameters (Sousa et al. 2008) is acceptable for other species. In other words, we expect that the slopes will be as small as possible.

We can see an example of this (star HD1461) in Fig. 3. We have chosen nickel because its lines cover a good range of both EP and RW, thus allowing a good determination of the slopes.

In Fig. 4, we plot the slopes of EP, obtained for every star, as a function of the stellar parameters (T_{eff}, $\log g$, ξ_t and [Fe/H]). From the analysis of the plots, we can see no discernible trends except in the case of the T_{eff} plot, where we observe that cooler stars ($T_{eff} \lesssim 5000$ K) have a systematic bias away from the expected values. A higher dispersion is also seen, on average, for cooler stars. This might be due to the stronger line blending in cooler stars as well as to the fact that the computed $\log gf$ values (derived from the solar spectrum) may not be adequate for these stars. The same effect was noticed in the RW plots.

We have also plotted the [CrI/CrII] value as a function of the stellar parameters in order to ensure that the ionisation equilibrium that was forced to the FeII lines (Sousa et al. 2008) was acceptable to other elements. This is depicted in Fig. 5. We expect that [CrI/CrII] will be independent of these parameters.

Table 3. Sample table of the derived abundances of the elements, rms and number of measured lines (n) for each star.

Star ID	[Si/H]	rms	n	[Ca/H]	rms	n	[ScI/H]	rms	n	[ScII/H]	rms	n	...
...	...	...	...	...	...	...	...	...	...	...	...	...	...
HD12617	0.15	0.10	17	0.05	0.14	10	0.48	0.31	3	0.14	0.11	6	...
HD13060	0.06	0.07	16	0.03	0.06	12	0.12	0.11	3	-0.01	0.05	6	...
HD13724	0.24	0.02	17	0.22	0.02	11	0.30	0.02	3	0.31	0.07	6	...
HD13789	-0.04	0.08	16	0.01	0.12	11	0.31	0.25	3	-0.13	0.13	6	...
HD13808	-0.14	0.07	16	-0.20	0.11	11	-0.05	0.11	3	-0.22	0.08	6	...
HD14374	-0.02	0.02	16	-0.03	0.04	11	0.00	0.05	3	-0.07	0.07	6	...
HD14635	0.02	0.10	18	0.05	0.14	11	0.49	0.30	3	-0.04	0.11	6	...
HD14680	-0.16	0.05	17	-0.12	0.11	12	-0.01	0.12	3	-0.21	0.07	6	...
HD14744	-0.11	0.04	18	-0.13	0.06	11	0.01	0.17	3	-0.15	0.08	6	...
HD14747	-0.24	0.01	17	-0.23	0.01	11	-0.22	0.03	3	-0.22	0.04	6	...
...	...	...	...	...	...	...	...	...	...	...	...	...	...

Table 4. Abundance sensitivities of the studied elements to changes in the stellar parameters (temperature with $\Delta T_{eff} = \pm 100$ K, surface gravity with $\Delta \log g = \pm 0.3$ dex, metallicity with Δ[Fe/H] $= \pm 0.3$ dex, and microturbulence with $\Delta \xi_t = \pm 0.5$ km s^{-1}).

Star ID	T_{eff} [K]	$\log g$	[Fe/H]	ξ_t [km s^{-1}]	Na	Mg	Al	Si	Ca	ScI	ScII
Temperature with $\Delta T_{eff} = \pm 100$ K											
HD10567	4748	4.42	-0.02	0.90	± 0.10	± 0.02	± 0.07	∓ 0.06	± 0.12	± 0.14	∓ 0.02
HD20616	5519	4.43	0.01	0.94	± 0.06	± 0.06	± 0.05	∓ 0.01	± 0.08	± 0.10	∓ 0.01
HD20945	6118	4.50	0.03	1.21	± 0.06	± 0.06	± 0.05	± 0.03	± 0.07	± 0.09	± 0.01
Surface gravity with $\Delta \log g = \pm 0.3$ dex											
HD19556	5676	4.03	0.06	1.11	∓ 0.05	∓ 0.05	∓ 0.02	± 0.01	∓ 0.05	∓ 0.01	± 0.13
HD11720	5667	4.32	0.22	1.01	∓ 0.07	∓ 0.06	∓ 0.02	± 0.01	∓ 0.07	∓ 0.01	± 0.12
HD20260	5658	4.49	0.18	1.02	∓ 0.07	∓ 0.06	∓ 0.02	± 0.01	∓ 0.08	∓ 0.01	± 0.12
Microturbulence with $\Delta \xi_t = \pm 0.5$ km s^{-1}											
HD9828	5381	4.42	-0.26	0.64	∓ 0.02	∓ 0.03	∓ 0.02	∓ 0.01	∓ 0.07	∓ 0.02	∓ 0.06
HD18956	5726	4.41	-0.24	0.95	∓ 0.02	∓ 0.04	∓ 0.01	∓ 0.01	∓ 0.08	∓ 0.01	∓ 0.07
HD4444	5999	4.37	-0.22	1.26	∓ 0.02	∓ 0.03	∓ 0.01	∓ 0.02	∓ 0.08	∓ 0.01	∓ 0.09
Metallicity with Δ[Fe/H] $= \pm 0.3$ dex											
HD7874	5778	4.46	-0.67	1.03	∓ 0.03	± 0.00	∓ 0.01	± 0.01	± 0.00	∓ 0.01	± 0.06
HD9670	5845	4.39	-0.18	1.04	± 0.00	± 0.01	∓ 0.01	± 0.02	± 0.00	∓ 0.01	± 0.08
HD20220	5757	4.47	0.29	1.01	± 0.04	± 0.03	± 0.01	± 0.05	± 0.03	± 0.01	± 0.11

Star ID	T_{eff} [K]	$\log g$	[Fe/H]	ξ_t [km s^{-1}]	TiI	TiII	V	CrI	CrII	Mn	Co	Ni
Temperature with $\Delta T_{eff} = \pm 100$ K												
HD10567	4748	4.42	-0.02	0.90	± 0.14	∓ 0.02	± 0.15	± 0.09	∓ 0.08	± 0.06	± 0.02	∓ 0.02
HD20616	5519	4.43	0.01	0.94	± 0.12	∓ 0.01	± 0.12	± 0.08	∓ 0.04	± 0.07	± 0.06	± 0.05
HD20945	6118	4.50	0.03	1.21	± 0.09	± 0.01	± 0.10	± 0.08	∓ 0.02	± 0.07	± 0.07	± 0.06
Surface Gravity with $\Delta \log g = \pm 0.3$ dex												
HD19556	5676	4.03	0.06	1.11	∓ 0.01	± 0.12	∓ 0.01	∓ 0.02	± 0.11	∓ 0.02	± 0.01	± 0.01
HD11720	5667	4.32	0.22	1.01	∓ 0.01	± 0.12	∓ 0.01	∓ 0.03	± 0.11	∓ 0.05	± 0.03	± 0.01
HD20260	5658	4.49	0.18	1.02	∓ 0.02	± 0.12	∓ 0.01	∓ 0.04	± 0.11	∓ 0.04	± 0.02	± 0.02
Microturbulence with $\Delta \xi_t = \pm 0.5$ km s^{-1}												
HD9828	5381	4.42	-0.26	0.64	∓ 0.08	∓ 0.06	∓ 0.03	∓ 0.06	∓ 0.07	∓ 0.07	∓ 0.05	∓ 0.05
HD18956	5726	4.41	-0.24	0.95	∓ 0.03	∓ 0.08	∓ 0.01	∓ 0.06	∓ 0.09	∓ 0.04	∓ 0.03	∓ 0.03
HD4444	5999	4.37	-0.22	1.26	∓ 0.03	∓ 0.08	∓ 0.01	∓ 0.04	∓ 0.12	∓ 0.04	∓ 0.03	∓ 0.03
Metallicity with Δ[Fe/H] $= \pm 0.3$ dex												
HD7874	5778	4.46	-0.67	1.03	∓ 0.01	± 0.06	∓ 0.01	∓ 0.01	± 0.04	∓ 0.01	± 0.00	± 0.00
HD9670	5845	4.39	-0.18	1.04	∓ 0.01	± 0.07	∓ 0.01	∓ 0.01	± 0.06	± 0.00	± 0.01	± 0.02
HD20220	5757	4.47	0.29	1.01	± 0.00	± 0.11	± 0.01	± 0.02	± 0.08	± 0.03	± 0.03	± 0.05

As seen in Fig. 5, there is a divergence of the expected ratio for stars with $T_{eff} < 4900$ K. We cannot discern any significant trend on the plots of the other parameters. This result, together with the one found for Ni, raises some doubts on the abundance values derived for stars with lower temperatures ($T_{eff} \lesssim 4900$ K).

Finally, we plotted the abundance ratios [X/Fe], as a function of the stellar parameters. We did not find any relevant trends except on the T_{eff} plot, represented in

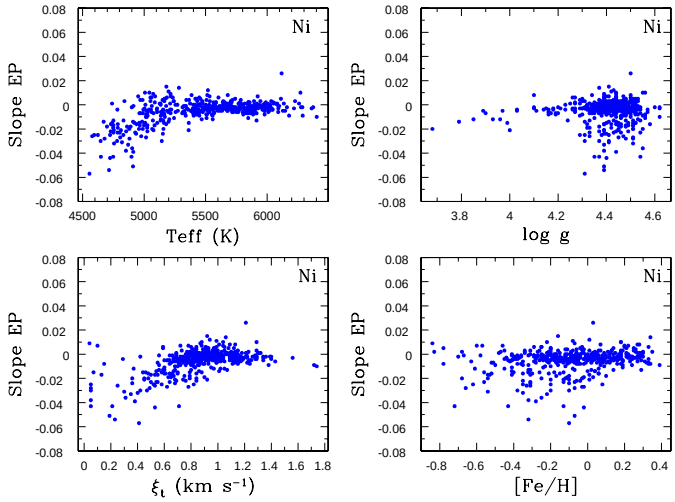

Fig. 4. EP slopes as a function of T_{eff}, $\log g$, ξ_t and [Fe/H] for Ni.

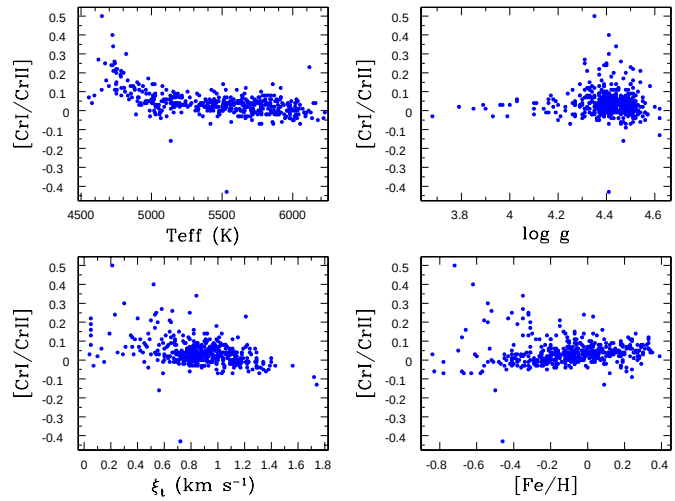

Fig. 5. Plots of [CrI/CrII] as a function of T_{eff}, $\log g$, ξ_t and [Fe/H].

Fig. 6. The slopes of [X/Fe] with T_{eff} per 1000 K are listed in Table 5.

We observe significative trends with T_{eff} for TiI, ScI, V, Co and Al. We can clearly see that the trend away from the expected value, except for Co and Al, is heavily influenced by the cooler stars, where the abundance might have been overestimated due to blending effects, to deviations from the excitation or ionisation equilibrium, or to problems associated with the differential analysis: we must not forget that the oscillator strengths were calculated for the Sun. In order to account for these effects we have decided to establish a cutoff temperature: $T_{cutoff} = 5000$ K for TiI, $T_{cutoff} = 5100$ K for ScI and $T_{cutoff} = 5300$ K for V. Only stars above this temperature will be considered in the remaining of this paper, for the aforementioned elements. We shall note this when we analyse the results.

Table 5. Slopes of [X/Fe] ratio as a function of T_{eff} per 1000K

Species	Slope(T)±rms	Species	Slope(T)± rms
Si	-0.004±0.051	CrI	-0.053±0.026
TiI	-0.192±0.081	CrII	0.039±0.048
TiII	0.062±0.076	Co	-0.128±0.067
ScI	-0.269±0.128	Ni	-0.012±0.034
ScII	0.050±0.065	Na	-0.017±0.066
Ca	-0.045±0.069	Mg	-0.009±0.089
Mn	-0.034±0.093	Al	-0.161±0.080
V	-0.452±0.086		

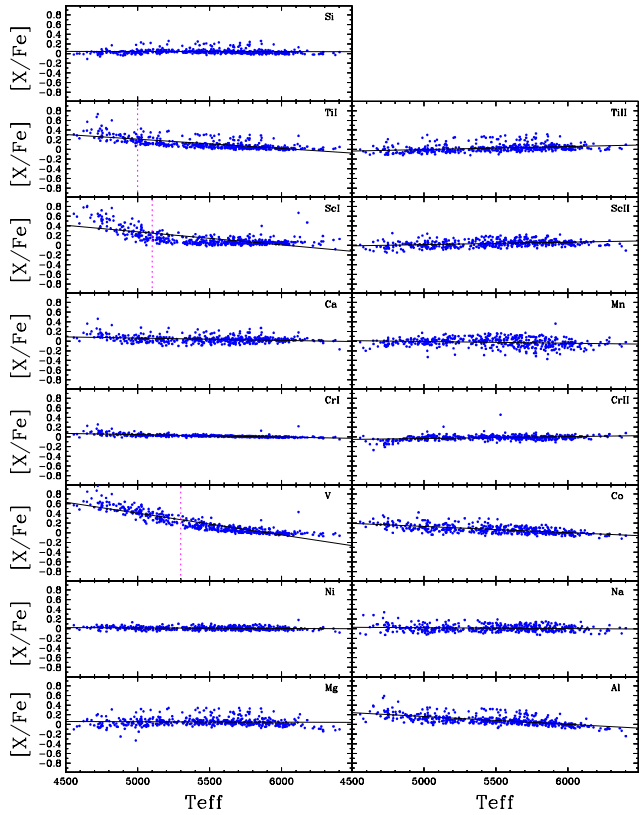

Fig. 6. [X/Fe] vs. T_{eff} plots. The dots represent the stars of the sample. The solid lines depict the linear fits of the data. The vertical purple dotted lines indicate the cutoff temperature when appropriate.

4.2. Comparison of the abundances with the literature

In order to test the reliability of our results, we made a comparison of the derived abundances with the ones obtained by Bensby et al. (2005), Valenti & Fischer (2005), Gilli et al. (2006) and Takeda (2007), for common stars, as seen in Fig. 7. This way, it is possible to make a qualitative verification of any systematic errors in our abundance determinations.

We can see that, in general, our results agree with the [X/H] obtained by other authors. However, we observe a systematic underabundance trend in Ca, CrI (Gilli et al. 2006) and Ti (Valenti & Fischer 2005) and a systematic overabundance trends in Mn (Gilli et al. 2006), Mg and Al (Gilli et al. 2006; Bensby et al. 2005). It's worth mention-

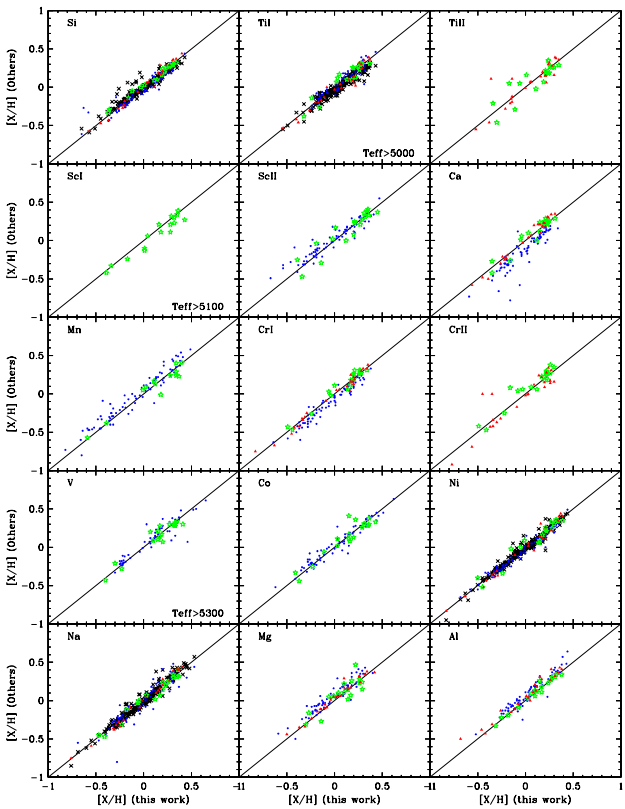

Fig. 7. Comparison of the derived abundances with those listed by other authors: Bensby et al. (2005) (red triangles), Valenti & Fischer (2005) (black crosses), Gilli et al. (2006) (blue dots) and Takeda (2007) (green stars). The elements are identified in the top left corner of each plot.

ing the existence of a population of stars with a systematic underabundance in Si (Valenti & Fischer 2005) and we have verified that this is not a planet host population. We do not know the origin of these differences. In general, though, the differences are small and systematic, meaning that, from a relative point of view, all studies agree very well.

5. Abundances in planet-hosts

Although we have a relatively small number of planet host stars (**68**), this number is enough to observe if there are any discernible differences in the abundances of stars with and without planets.

We must note that five planet host stars (HD4308, HD27894, HD111232, HD114729 and HD330075) are considered to belong to the thick disk. This means that approximately 7% of the planet host stars in our sample belong to the thick disk and that approximately 17% of the thick disk stars are planet hosts. These values must be regarded as lower limits, since (some?, most?) planets (may?) still be awaiting confirmation in the whole sample. **Is is important to note that there was no known bias in the selection of the thick disk stars of this sample regarding the existence of planets**.

5.1. The [X/H] Distributions

The [X/H] distributions of planet and non-planet hosts are depicted in Fig. 8. The stars with and without planets as well as the stars only with neptunes and super-earths[6] are represented by a dashed blue, solid red, and dotted black line, respectively. The vertical lines on the top of each histogram represent their average value.

We can observe a clear metallicity excess for giant planet-host stars for all the elements in study. These results are in good agreement with previous similar studies (e.g. Bodaghee et al. 2003; Beirão et al. 2005; Gilli et al. 2006; Bond et al. 2006; Takeda 2007). Our results are also consistent with previous studies of iron abundances (e.g. Gonzalez 1998; Gonzalez et al. 2001; Laws et al. 2003; Santos et al. 2001, 2003, 2004, 2005; Fischer & Valenti 2005), as expected. Interestingly, we also found that thick disk stars with planets are more metal-rich ($<$[Fe/H]$>$ = -0.15) than "single" stars ($<$[Fe/H]$>$ = -0.34).

Table 6 lists the average values of [X/H] along with their rms**, the number of stars used in their determination**, and the difference of averages between stars with and without planets. These differences range from 0.16 for Al to 0.25 for Mn. The last **four** columns list the average [X/H] ratio of neptunian hosts and hosts with neptunes and super-earths only**, along with the number of stars used in their determination.**

The difference of the average abundance between stars with and without giant planets is, on average, slightly below the figures of Bodaghee et al. (2003) and Gilli et al. (2006) by $\sim$ 0.03 dex, except for vanadium, in which our value is more than $\sim$ 0.05 dex higher. This difference is above the results of Bond et al. (2006) for all elements. Our results are very similar to the ones of Takeda (2007). The dispersion of this difference is the smallest among all authors, likely attesting the quality of our results.

It is interesting to see that in most histograms (except for Mg) the distributions of the abundances in planet host stars are not symmetrical: there is an increase of [X/H] up to a maximum and shortly after there is a huge cutoff in distribution. This cutoff is located at [X/H] $\sim$ 0.3 for Ca and CrII, [X/H] $\sim$ 0.4 for Si, TiI, TiII, ScI, ScII, CrI, Ni, Na, Mg, and Al and [X/H] $\sim$ 0.5 for Mn, V, and Co. The cutoff might suggest that we are looking at the metallicity limit of the solar neighbourhood stars (e.g. Santos et al. 2003), as most of the planet hosts are at the high metallicity end of the sample.

Some planet host distributions seem to be slightly bimodal (Mn, V, and Na). We do not know the cause of this effect. It might be due only to small number statistics.

Regarding the stars with only neptunian planets (N=3), we can observe that they have the smallest [X/H] mean value for every element. The mean [X/H] values of ScI, TiI, V, Mg, and Al are very close to the mean values of the non planet host stars. We must note that we

[6] HD4308, HD40307, HD69830, HD47186, HD160691 and HD181433. The first three stars host neptunians and super-earth type planets only.

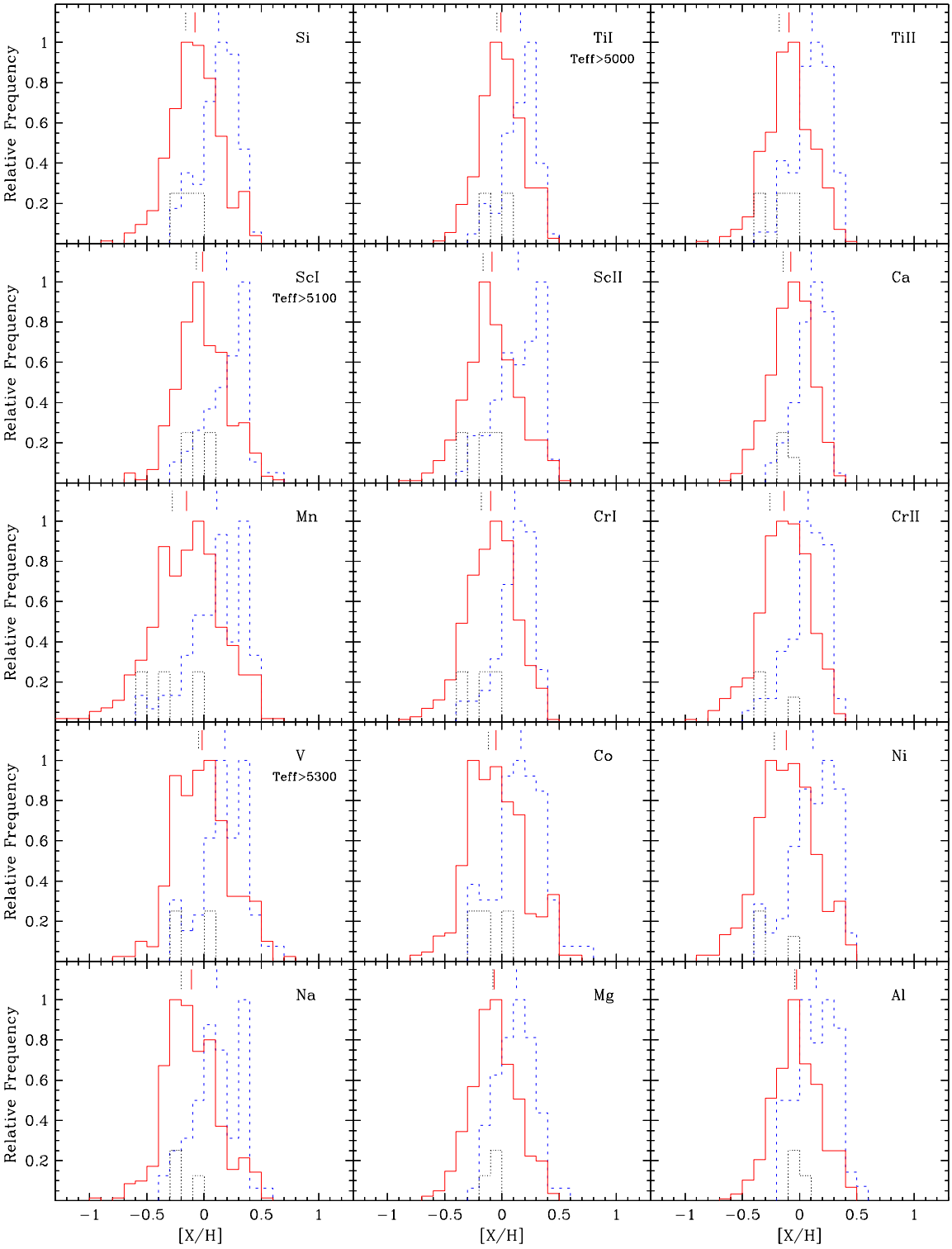

Fig. 8. [X/H] distribution of the different elements. The stars with and without planets are represented by a dashed blue, and solid red line respectively. The stars that exclusively host neptunians and super earth-planets are represented by a black dotted line. The mean value is pictured by a dashed (with planets), solid (without planets), and dotted (neptunian and super earth hosts only) vertical lines on the top of each distribution. The neptunian and super-earth distribution was set smaller for clarity.

only have 3 stars that only have neptunes and 3 stars that are neptunian and jovian hosts. Therefore, any results regarding the neptunian and super-earth planet hosts must be seen as very preliminary. Despite that, the values for the neptunian and super-earth only hosts confirm that the probability of finding one of these planets may even

Table 6. Average abundance values for stars with and without planets, along with their rms**, the number of stars used in their determination**, and the difference between the two groups. The last **four** columns list the average abundance values of neptunian hosts and hosts with neptunes and super-earths only**, along with the number of stars used in their determination.**

Species	Planet hosts			Non-planet hosts			Difference	**Neptunian hosts**		Neptunian hosts only	
(X)	⟨[X/H]⟩	rms	**N**	⟨[X/H]⟩	rms	**N**	of Averages	⟨[X/H]⟩	**N**	⟨[X/H]⟩	**N**
Si	0.13	0.17	68	-0.08	0.21	383	0.21	0.08	6	-0.16	3
TiI	0.16	0.14	62	-0.01	0.18	321	0.17	0.12	4	-0.05	2
TiII	0.11	0.15	68	-0.09	0.20	383	0.20	0.04	6	-0.18	3
ScI	0.20	0.19	61	-0.01	0.22	288	0.21	0.14	4	-0.07	2
ScII	0.14	0.19	68	-0.09	0.23	383	0.23	0.12	6	-0.17	3
Ca	0.10	0.14	68	-0.08	0.18	383	0.18	0.05	6	-0.14	3
Mn	0.11	0.24	68	-0.15	0.31	383	0.27	0.05	6	-0.28	3
CrI	0.11	0.17	68	-0.10	0.22	383	0.21	0.06	6	-0.18	3
CrII	0.07	0.17	68	-0.14	0.22	383	0.21	-0.01	6	-0.26	3
V	0.18	0.20	56	-0.02	0.25	243	0.20	0.15	4	-0.05	2
Co	0.17	0.21	68	-0.05	0.25	383	0.22	0.19	6	-0.12	3
Ni	0.12	0.20	68	-0.12	0.24	383	0.23	0.07	6	-0.22	3
Na	0.11	0.20	68	-0.11	0.23	383	0.22	0.10	6	-0.20	3
Mg	0.13	0.16	68	-0.07	0.20	383	0.19	0.12	6	-0.08	3
Al	0.15	0.17	68	-0.03	0.20	383	0.17	0.17	6	-0.04	3
Fe*	0.10	0.17	68	-0.12	0.23	383	0.22	0.03	6	-0.24	3

* [Fe/H] values from Sousa et al. (2008).

be higher in metal poor stars and they seem to present a very different trend from the jovian host stars. Our results for stars hosting only neptunian-like planets are in agreement with those found by Udry et al. (2006, 2007) and Sousa et al. (2008) for [Fe/H].

Fig. 9 illustrates the [X/H] distribution in a different perspective: the histograms of the number of stars with planets relative to the total number of stars of each bin (0.1 dex). We can observe that there is a general increase in the percentage of stars with planets for all elements, with increasing [Fe/H], after a low metallicity plateau. This observation is in agreement with the findings of other authors like, for example, Santos et al. (2001, 2004), and Fischer & Valenti (2005) for [Fe/H].

5.2. *The [X/Fe] versus the [Fe/H] plots: stars with and without planets*

The [X/Fe] vs. [Fe/H] plots are traditionally used to study the chemical evolution of the galaxy as well as to identify its different stellar populations (thin disk, thick disk, halo), which have distinct abundance ratios (see e.g. Bensby et al. 2003, Fuhrmann 2004). In this subsection, we will analyse them only to observe if there are any differences in the abundance of stars with and without planets, for the same value of [Fe/H].

Fig. 10 shows the [X/Fe] values for the two samples as a function of [Fe/H]. The blue triangles and the red circles represent stars with and without planets, respectively. The red dashed lines target the solar value. The used cutoff temperature is indicated when appropriate (see subsection 4.1.2).

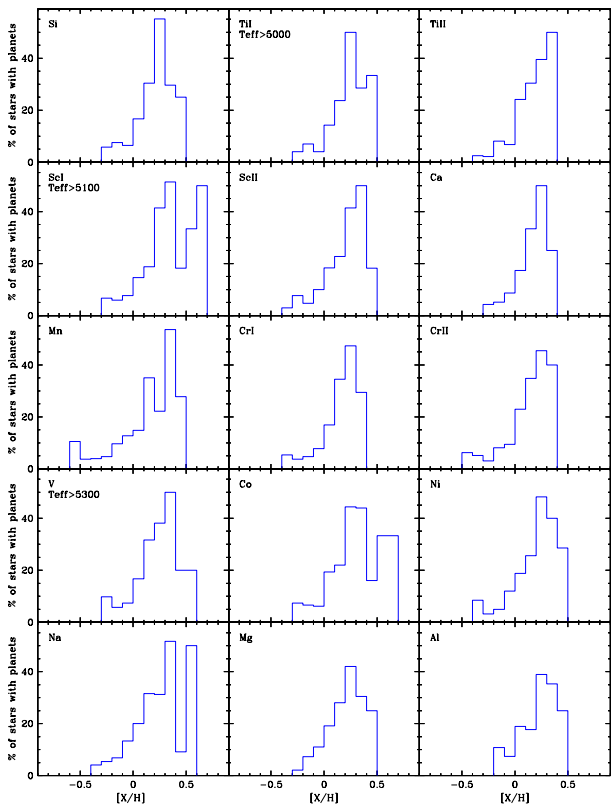

Fig. 9. Percentage of stars with planets as a function of [Fe/H]. The element label and the used cutoff temperature (when required) are located at the upper left corner of each plot.

The plots do not show any clear differences between the stars with and without planets for a given [Fe/H] value. We also did a Kolmogorov-Smirnov (KV) test of

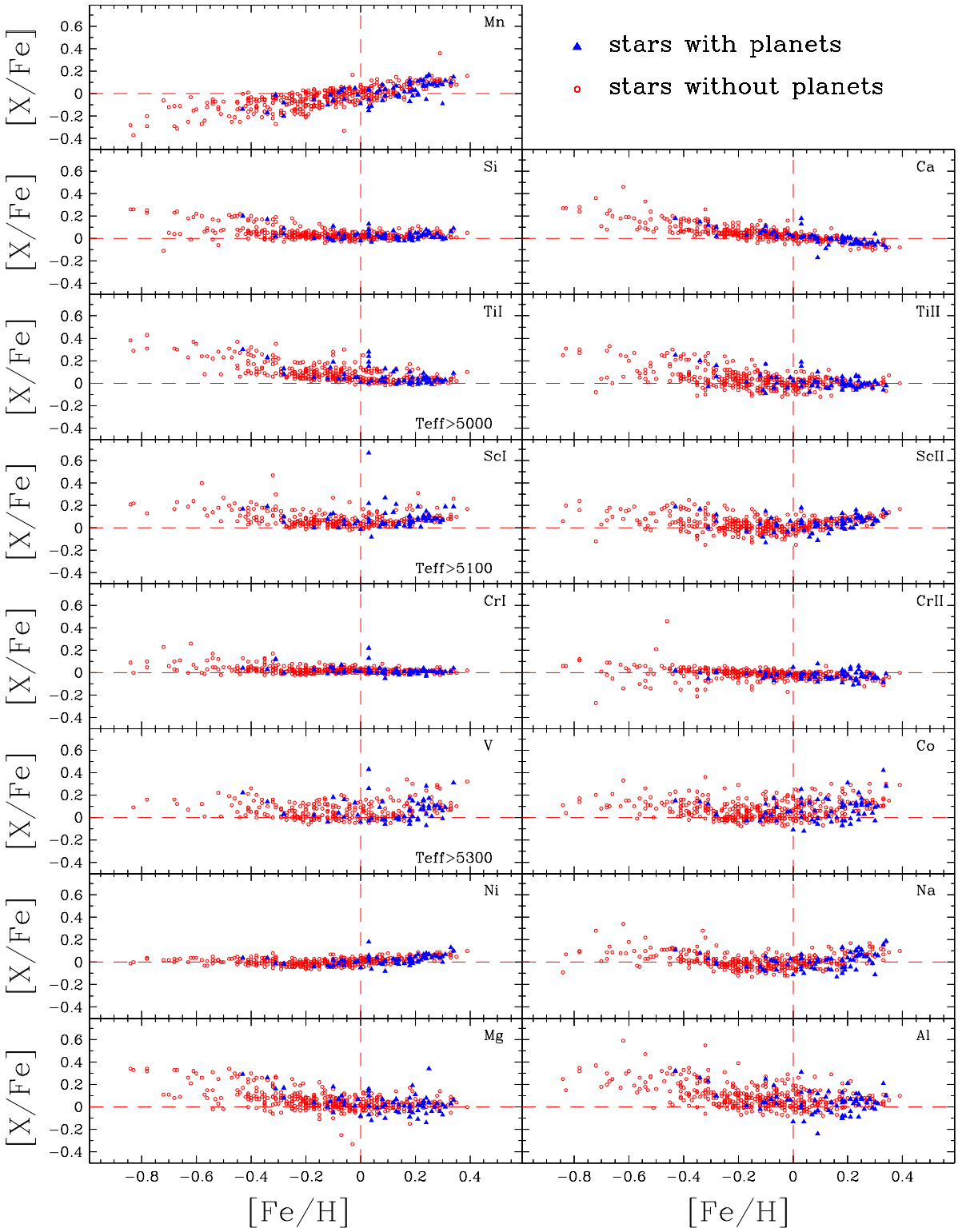

Fig. 10. [X/Fe] vs. [Fe/H] plots for the elements in study. The blue triangles and the red circles represent the stars with and without planets, respectively. The intersection of the dashed lines indicate the solar value. Each element is identified in the upper right corner of the respective plot and the cutoff temperature is indicated in the lower right corner when appropriate.

the [X/Fe] distributions for [Fe/H] > 0 without finding any significative differences between the planet host and the non planet host populations. The results generally agree with previous similar studies like, for instance, Gonzalez et al. (2001), Takeda et al. (2001), Sadakane et al. (2002), Bodaghee et al. (2003), Beirão et al. (2005), Fischer & Valenti (2005), Gilli et al. (2006) and Takeda (2007). This gives us confidence in our results.

Table 7. Average abundance values for the stars from the thin disk, transition and thick disk populations with [Fe/H] < 0, along with their rms. The last two columns depict the difference of the average abundance and the KS probabilities between the thin and the thick disk populations.

Species	Thin Disk		Intermediate		Thick Disk		Difference	KS
(X)	⟨[X/Fe]⟩	rms	⟨[X/Fe]⟩	rms	⟨[X/Fe]⟩	rms	of Averages	probability
Si	0.04	0.04	0.10	0.07	0.14	0.08	0.10	2.9e-09
TiI	0.10	0.07	0.19	0.10	0.22	0.11	0.12	6.7e-06
TiII	0.03	0.07	0.13	0.10	0.19	0.09	0.16	2.7e-11
ScI	0.07	0.06	0.14	0.11	0.15	0.07	0.08	1.5e-06
ScII	0.02	0.06	0.11	0.07	0.14	0.07	0.12	2.1e-11
Ca	0.06	0.06	0.12	0.12	0.14	0.07	0.08	8.9e-07
Mn	-0.05	0.07	-0.12	0.12	-0.17	0.08	0.12	5.6e-10
CrI	0.03	0.04	0.04	0.06	0.03	0.03	0.00	6.5e-01
CrII	-0.01	0.05	0.01	0.06	0.04	0.10	0.05	2.7e-05
V	0.05	0.06	0.10	0.07	0.11	0.08	0.06	3.1e-03
Co	0.05	0.08	0.11	0.09	0.10	0.06	0.05	8.3e-05
Ni	-0.01	0.03	0.02	0.02	0.02	0.03	0.03	2.6e-04
Na	-0.00	0.06	0.06	0.09	0.06	0.06	0.06	6.1e-07
Mg	0.05	0.08	0.17	0.10	0.21	0.11	0.16	2.1e-09
Al	0.10	0.10	0.21	0.14	0.22	0.09	0.12	8.8e-06

The reported cases of potential trends described by other authors like, for instance, Sadakane et al. (2002) for vanadium and cobalt, Bodaghee et al. (2003) for Ti, Mn, V and Co, Gilli et al. (2006) for V, Co, Mg and Al were not found. Robinson et al. (2006) claim to have found clear and significant overabundances of [Si/Fe] and [Ni/Fe]. Gonzalez & Laws (2007) have also found that there are strong indications that Al and Si abundances are systematically smaller for the planet host stars in the higher metallicity region, that the Ti abundance shows the opposite trend and hinted that the abundances of Na, Mg, Sc and Ni might have some differences between planet hosts and non planet hosts. We did not find any of these trends clear in our data.

In order to avoid systematic errors, we also did the analysis only for stars with $T_{eff} = T_{\odot} \pm 300$ K. These plots allow us to have a more accurate picture of the trends and differences among the two groups of stars: in a differential analysis like this one, the closer the star temperature is to the solar temperature, the more accurate, in average, the derived abundance is. A KS test was also done for the [X/Fe] distribution of this temperature restricted population. We did not find any new trend.

Some outliers may however exist in our sample. In all cases, the abnormal abundances may be explained by their high dispersion in individual lines abundances, by a high value of EP and/or RW slopes - see subsection 4.1.2, or due to non-LTE systematic effects for the highest temperature stars.

We have not found any abundance anomalies in the stars previously described in the literature: the underabundance of Ca in HD209100 derived by Bodaghee et al. (2003) and the overabundance of Mg and Al in the host star HD168746 described by Sadakane et al. (2002), Laws et al. (2003) and Gilli et al. (2006) was not found.

6. Thin and Thick disk

In this section we will perform a detailed analysis of the [X/Fe] distributions of three different populations: thin disk, thick disk, and the intermediate population, for [Fe/H] below the solar value. Above [Fe/H] > 0 we did not find any clear difference between thin and thick disk stars. The chosen criteria to select the stars of each population and the necessary data to calculate them were described in subsection 2.1. We must note that we only have 6 thick disk stars with [Fe/H] above the solar value. HD27894 is the thick disk member with the highest metal content, approximately 0.2 dex.

6.1. The [X/Fe] Distributions

The [X/Fe] distributions for [Fe/H] < 0 are depicted in Fig. 11. Each element and ion is identified on the top left corner of the plots, along with the used cutoff temperature when relevant. The solid red, dotted black and dashed blue lines represent the thin, intermediate and thick disk populations, respectively. The mean value of each population is depicted by the vertical lines above the distributions.

Table 7 lists the average values of [X/Fe] of the three populations along with their rms. The last two columns depict the difference of the average abundance and the KS probabilities between the thin and the thick disk populations.

From the analysis of the histograms and its associated table, we can observe that in the metallicity domain [Fe/H]<0, thick disk stars present higher average [X/Fe] values for most of the species. However, for CrI, there is no difference between the two populations and for Co and Ni this difference is very small (0.03 and 0.04 dex respectively). We can also see that for all elements there is at least a partial superposition between the thin and the

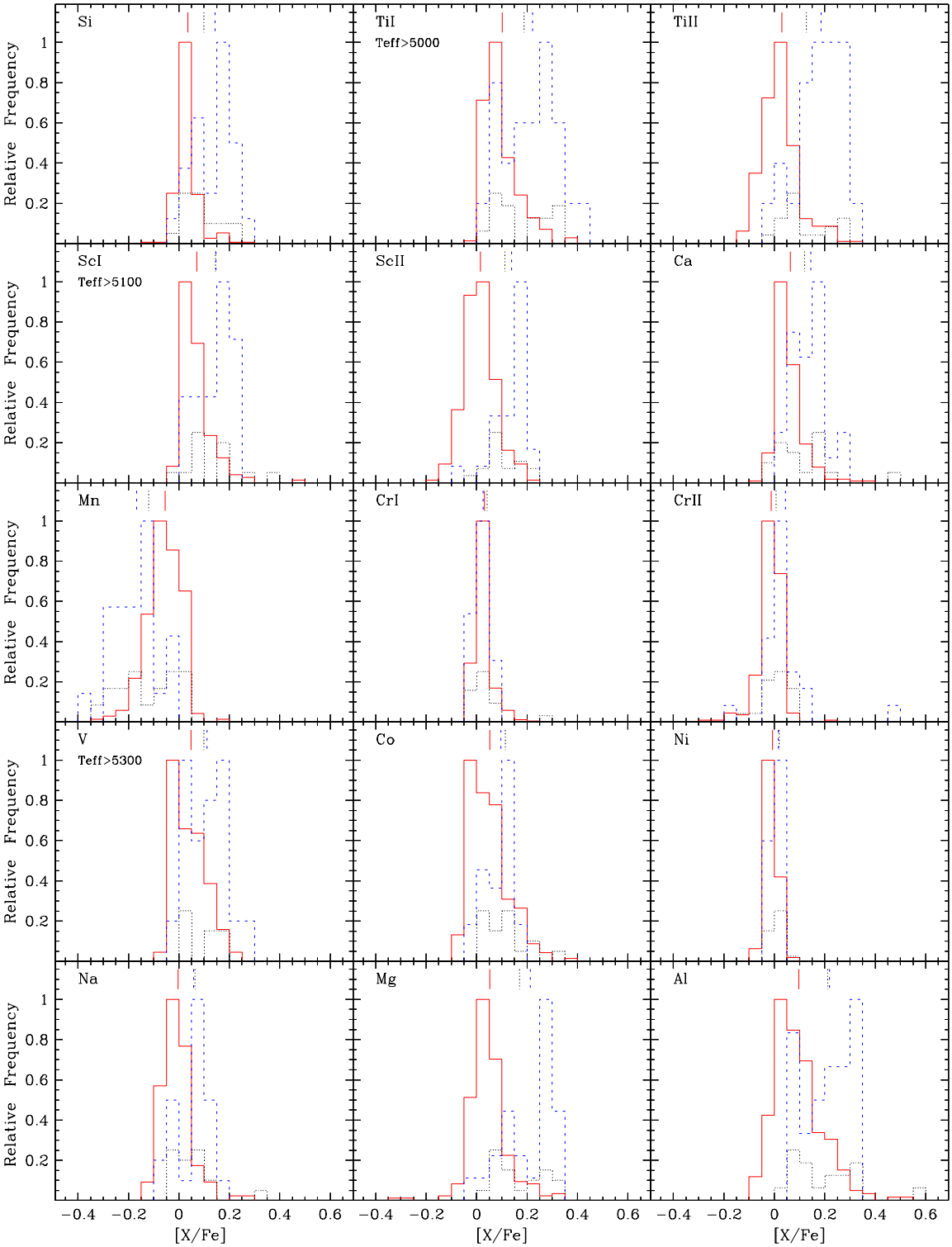

Fig. 11. [X/Fe] distributions of the species for [Fe/H]< 0. Each element and ion is identified on the top left corner of the plots, along with the used cutoff temperature when relevant. The solid red, dotted black and dashed blue lines represent the thin, intermediate and thick disk populations, respectively. The dotted black histogram was set smaller for clarity. The mean value is depicted by the vertical lines above each distribution, corresponding to the respective populations.

thick disk populations. The manganese histograms also present a different trend when compared with the remaining elements: the values of thin and thick disk populations invert, and, this time, the thick disk has an underabundance relative to the thin disk. The difference between both populations in this element is 0.12 dex. The

K-S probabilities tell us that all the stars from the thick and the thin disk are indeed from separate groups, with the exception of CrI which has a 65% probability that they belong to the same population. We note that the results based on CrII data are different from the CrI ones. However, CrII only presents two or three lines and, therefore, its results might be subjected to more biases. The mean values of the transition population are situated between those of the other populations, but its average oscillates somehow for some elements. It is difficult to conclude anything about the origin of this intermediate population. This is also valid for any statistical feature of the transition or the thick disk populations that might appear in the histograms: their statistics are too small. Nevertheless, we can observe that most thick disk histograms appear to be bimodal (Si, TiI, TiII, Ca, Mn, V, Co, Na, Mg, and Al): this may indicate that there are two populations in the thick disk with distinct [X/Fe] values. **On the other hand, however, the observed behaviour may simply be due to the fact that some stars from the thin disk are misclassified as thick disk stars: in every histogram of the aforementioned elements (except Mn), the lower [X/fe] mode of the thick disk histogram (that corresponds roughly to the peak of the thin disk histogram) has a much lower typical $P_{thickdisk}/P_{thindisk}$ than the stars of the higher [X/Fe] mode.**

With these results we confirm that the thin and the thick disk populations are chemically and statistically distinct (at least in the region below solar metallicity). Besides the differences already discovered by Fuhrmann et al. (1998) for Mg and by Bensby et al. (2003) for Si, Ca, Ti and Al, we also found that Sc, Mn, Co and Na show the same separation between the aforementioned populations. The results of Bensby et al. (2005) for Na are different from ours: in this element they found that the thin disk stars might be more abundant that the thick disk ones. We find the opposite trend. Regarding Ni, we can only say that there is a hint, also detected by Bensby et al. (2003), that the thick disk stars might be more abundant than thin disk stars at [Fe/H] < 0.

6.2. The [X/Fe] vs the [Fe/H] plots: thin and thick disk populations

The [X/Fe] vs the [Fe/H] plots are depicted in Fig. 12 and 13. The blue, black crossed and empty red circles represent the thick disk, transition and thin disk stars, respectively. The dashed lines mark the solar value. In Fig. 13 only stars with $T_{eff} \pm 300K$ are shown: this will allow us to have a better picture of the trends of the two groups.

Following the results of the [X/Fe] distributions, in Fig. 11, we verify that, in the [X/Fe] vs [Fe/H] plots, the abundance difference between the thin and thick disk populations is not clearly defined. We can observe that, for [Fe/H] < 0, the thin and the thick disk populations are mixed and for a fixed [Fe/H], we cannot conclude that the populations are fully separated. Instead, for the α elements (Si, Ca, Ti and Sc) and magnesium, the plots reveal a bifurcation of two different groups of stars, containing members from the three considered populations, that converge at [Fe/H] between -0.2 dex and the solar value. There are some hints that this might also be the case for V, Co, Na, and Al. These trends are clearer in Fig. 13. The slope of the branch with the higher [X/H] is always steeper than the slope of the lower branch. This means that the change in the [X/H] ratio of the higher branch is faster for [Fe/H] below the solar value.

We have not found any differences between the planet and non planet hosts among the thick disk members for a given [Fe/H] value. **We also did not find any strong prevalence of metal poor ([Fe/H] $\leqslant -0.2$) planet host stars in the thick disk, as suggested by Haywood (2008). However, we must note that we only have five stars under these conditions: two stars from the thin disk and three stars belonging to the thick disk. Therefore, we cannot conclude anything regarding the validity of Haywood (2008) result.**

Bensby et al. (2003, 2005) concluded that there is a clear separation between stars from the thick and the thin disk populations. However, we have not found this feature on our results. No reference to the existence of the detected bifurcation was given. We do not know its origin.

6.3. The [X/Fe] vs the [Fe/H] plots: galactic chemical evolution

It is widely accepted that the chemical evolution of the galaxy is dominated by nucleosynthesis occurring in many generations of stars, with the exception of the lightest elements (McWilliam 1997). Here, we will use the [X/Fe] vs [Fe/H] relations, in Figs. 12 and 13, to study the chemical evolution of the galaxy, assuming that [Fe/H] can be used as a time variable. It is difficult to say if the heavy scatter found in some of the plots are cosmic or due to errors.

In these figures we consider the stars with and without planets as one group, but we distinguish stars from the thick and the thin disk as well as an intermediate group (see subsection 2.1). The analysis is done element by element and compared to other recent studies on chemical abundances between stars with and without planets, namely, Sadakane et al. (2002), Bodaghee et al. (2003), Beirão et al. (2005), Fischer & Valenti (2005), Gilli et al. (2006), Gonzalez & Laws (2007), and Takeda (2007), hereafter SAD, BOD, BEI, FV05, GIL, GZ07, and TAK, respectively, as well as other reference studies by Chen et al. (2000), Allende Prieto et al. (2004), and Bensby et al. (2005) (hereafter CH00, AP04, and BEN, respectively).

6.4. The alpha elements

It is believed that the alpha elements (Si, Ca, Ti and Sc in this study) are mostly produced in massive stars that

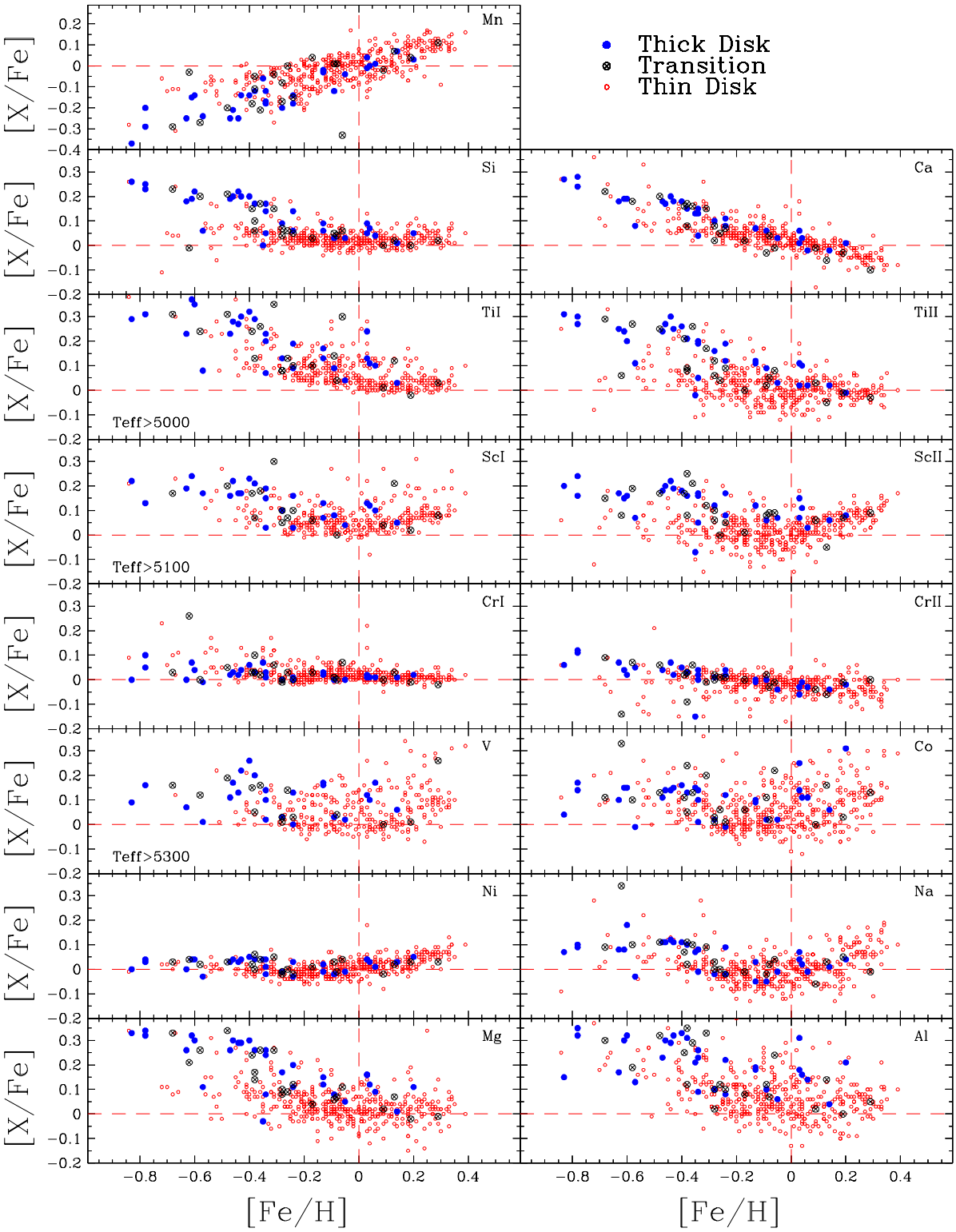

Fig. 12. [X/Fe] vs. [Fe/H] plots. The blue, black crossed and empty red circles represent the thick disk, transition and thin disk stars, respectively. The dashed lines mark the solar value. Each element is identified in the upper right corner of the respective plot and the cutoff temperature is indicated in the lower left corner when appropriate.

explode as type II supernova (SNe II), although type I supernova (SNe Ia) might also yield some of these elements (e.g. Thielemann et al. 2002).

We can observe that for all elements comprising this group, there is a bifurcation for [Fe/H] below solar. The upper branch descends from overabundances of ~ 0.3, 0.4 dex toward solar abundances at [Fe/H] around the solar

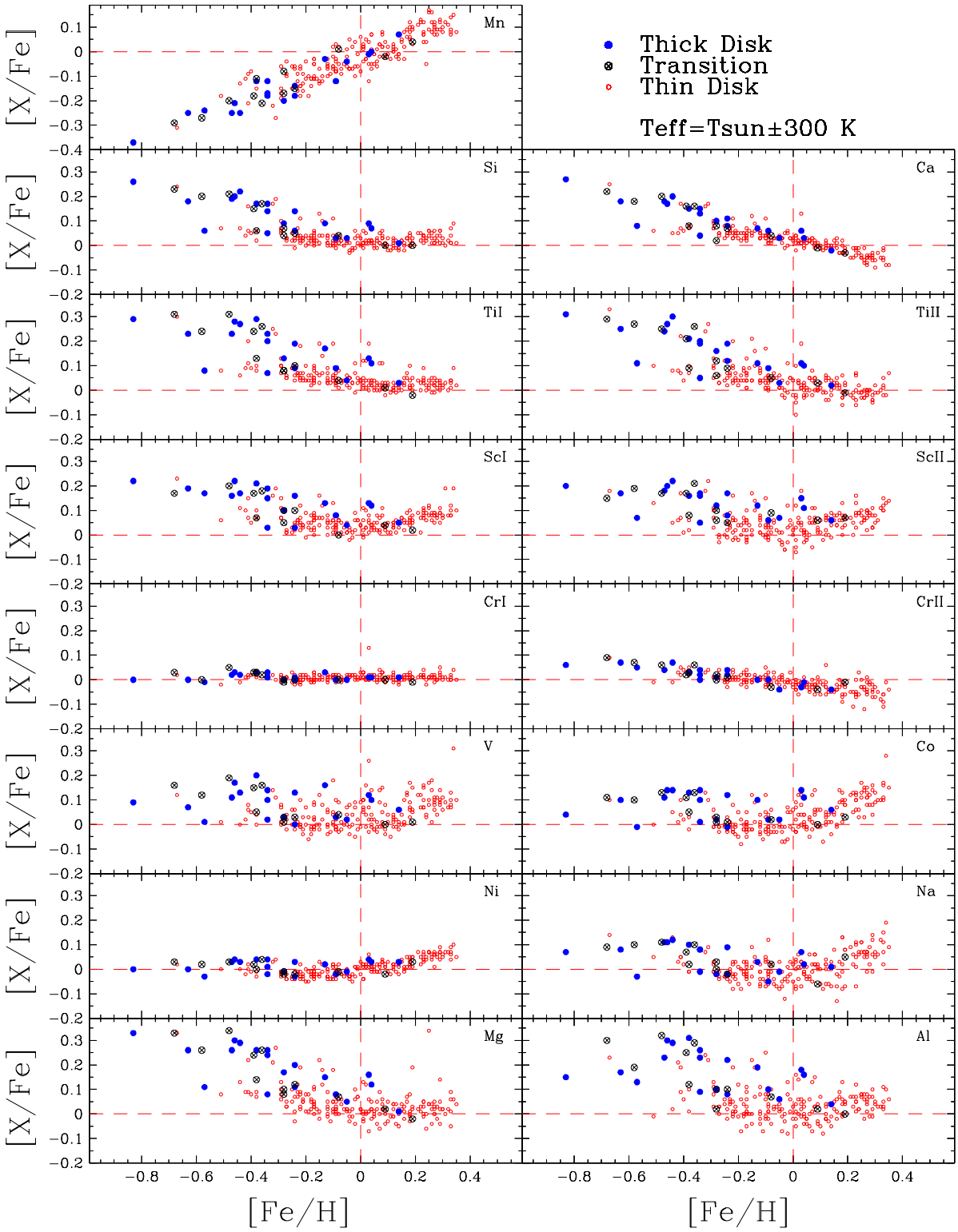

Fig. 13. Same as Fig. 12 but only with stars having $T_{eff} = T_{\odot} \pm 300$ K.

value, while the lower branch has a much slower descent. Then, the abundance remains at solar value and at some point it will ascend, descend or remain constant toward higher [Fe/H] values, depending on the element: this might be an observational evidence that the α elements are produced in different amounts by different SN (McWilliam 1997). We should note, however, that titanium has over-abundances relative to the other α elements at [Fe/H] below the solar value and that its slopes in this metallicity region are steeper than for calcium and silicon. The Sc abundances, for [Fe/H] < 0, seem to slowly decrease or

remain constant until [Fe/H] reaches ~ -0.3 dex, where it has a downturn toward solar values.

6.4.1. Silicon

We can see that there exists a clear bifurcation in a region of [Fe/H] ranging from -0.85 to 0.0 dex. This can be seen more clearly in Fig. 13. The [Si/Fe] value of the upper branch decreases until [Fe/H] ~ -0.2 dex, before joining with the lower branch, that has a much gentler descent. Then, the [Si/Fe] ratio remains constant at solar value, with a slight upward trend starting at [Fe/H] $\sim +0.2$.

The results of the other authors are similar to ours in general. However, the plateau described also in CH00 seems to start much earlier that in our case and in BEN it seems that there is no plateau. BOD, FV05 and GZ07 obtained slightly lower abundances ($\sim$ 0.05 dex) in the plateau region. The upward trend at [Fe/H] > 0 is not visible in SAD, FV05, GIL and TAK. The AP04 results are systematically above ours (more than $\sim +0.1$ dex) and the upward slope is much stronger than in our results. No author refers the observed bifurcation.

6.4.2. Calcium

Calcium shows an uniform downward trend in the entire metallicity range. It begins from abundance values of $\sim +0.3$ at [Fe/H] ~ -0.85 dex to [Ca/Fe] values of ~ -0.1 at [Fe/H] $\sim +0.4$, going through the solar value at solar [Fe/H]. The branches of the bifurcation are harder to observe and they seem to join at [Fe/H] ~ -0.3 dex. There might exist a slight plateau for solar abundance values in the region of metallicity from -0.2 to the solar value. This is more evident in Fig. 13.

The trends obtained for calcium are similar to most studies found in the literature, such as CH00, BOD, GIL, TAK and GZ07. However, the abundances obtained by SAD, AL4 and BEN do not continue to descend for [Fe/H] > 0. GIL and GZ07 results have the same trend as we see here, but the [Ca/H] values are systematically lower than ours. No one refers the bifurcation.

6.4.3. Titanium

The upper branch of both TiI and TiII plots decrease until [Fe/H] reaches $\sim$ 0.0-0.2 dex, where it joins to the lower branch. Then it settles there for the remainder of the [Fe/H] range, at solar [Ti/Fe] value. As the plots of Ti have considerable scatter it is easier to see the trends in Fig. 13. We can see that the higher branch population has a [Ti/Fe] from $\sim +0.35$ to ~ 0.0 dex, in a region of [Fe/H] ranging from -0.85 to ~ 0.0 dex.

A similar behaviour in the titanium trends is found in the studies of CH00, SAD, BOD, GIL, BEN, TAK and GZ07. However, the plateau region in BOD seem to be slightly below the solar value. The observed trend in FV05 has a continuously decreasing trend throughout all the [Fe/H] range. The data from AP04 shows an upturn in the [Ti/Fe] values above solar metallicity. We have not found the weak upturn in TiII reported by TAK. Again, no author refers the observed bifurcation.

6.4.4. Scandium

There is considerable scatter in the points in Fig. 12 for the Sc plot. The trend is easier to see in Fig. 13. In the ScI panel we can observe a very slow decrease in the abundance of both branches until they join at [Fe/H] ~ -0.1. Then it remains constant at the solar value in the region of $-0.1 \lesssim$ [Fe/H] $\lesssim +0.1$. There is then an increase of the abundance for [Fe/H] $\gtrsim +0.1$ dex. The ScII plot is similar to the ScI one, but is seems that there is no plateau: the [ScII/Fe] value just decreases until the [Fe/H] reaches the solar value and then it begins to increase toward the end of the [Fe/H] range.

The results of BOD, GIL and GZ07 are slightly different from ours. The results are similar for [Fe/H] < 0, but then we observe an increase of the abundance with [Fe/H] and they don't. However, BOD suggests that there might be an upswing for iron rich stars, but it is not conclusive due to scattering. This upswing is also noticed by GIL and GZ07, though it is elusive. Our figures suggest a much more evident trend. The results of SAD and TAK are similar to ours, although the ScI and ScII results of the latter do not show the upturn or show a very weak one for metallicity values above the solar value. AP04 also reports the same trends, but their results have a systematic overabundance when compared to ours. No branch is found in the referred works.

6.5. The iron peak elements

It is believed that the iron peak elements are mostly created in SNe Ia explosions (Thielemann et al. 2002). In our plots we can observe that CrI and Ni (for [Fe/H] < 0) follow in lockstep with iron which means that they should have the same origin. On the other hand, vanadium and cobalt have trends more similar to the α elements. Manganese seems to mirror the behaviour of the alpha elements.

6.5.1. Chromium

In the CrI plot, the chromium abundances are constant around the solar value, as expected by the theory. The scatter is small when compared to the other elements. We note that the CrII plot has a weak continuous downward trend but we only have 2 or 3 lines per star, which makes the abundance determination more subjected to blending effects or to some other unknown systematic error.

The CrI results of CH00, SAD, BOD, BEN, and TAK are similar to ours. However, we can observe a slight systematic underabundance in the results of BOD. The results of GIL for CrI suggest a downward trend similar to

the one of our CrII plot and their values have a systematic underabundance when compared to ours. Regarding our CrII plot, we find that it is different from the CrI plots of every author. The only work, beside ours, with a CrII determination is TAK: it shows a systematic upward trend throughout the metallicity range, in opposition to our results.

6.5.2. Vanadium

Vanadium has a behaviour similar to the alpha elements, which might indicate a common origin. However, we do not see a clear bifurcation, although there are some hints that it might exist (see Fig. 13). The [V/Fe] values slowly decline toward solar metallicity up to [Fe/H] ~ -0.1. Then, the trend inverts and we can observe an upswing toward the upper end of the [Fe/H] region. We can easily verify that there is a lot of scatter. We should note that the vanadium abundances were impossible to read if we had not removed the stars with $T_{eff} > 5300$ K (see subsection 4.1.2). Therefore, it is impossible to reach any important conclusion regarding the real trend or the origin of this particular element.

Our results for vanadium differ from CH00 and SAD: they report that vanadium mimics Cr and Ni. However, the results of BOD, GIL and TAK are similar to ours. Nevertheless, we should note that almost every author reports high levels of scattering. Some authors refer to NLTE effects (e.g. BOD, GIL) to explain it.

6.5.3. Cobalt

Cobalt has a large scatter throughout the entire metallicity range. The abundance value decreases very slowly until it reaches [Fe/H] ~ -0.1 dex. Then, the [Co/Fe] ratio remains constant around the solar value until [Fe/H] reaches the solar metallicity. Toward higher metallicities there is a slow but clear increasing trend. In Fig 13, the abundance seems to be constant all the way up to the solar value and a bifurcation similar to the α elements might also be present. Cobalt has similar trends to vanadium and to the alpha elements. This element might be subjected to NLTE effects (see subsection 4.1.2). Cobalt, as well as vanadium, are odd-Z nuclei but, despite of that, they have similar trends with the α elements.

The general trends observed by SAD, BOD, GIL and TAK are present in our plots. AP04 also presents a similar result. However, the upturn observed by AP04 for high [Fe/H] is steeper than those observed here. All abundance determinations, including ours, have considerable scatter. It is thus difficult to draw any strong conclusion from the analysis.

6.5.4. Nickel

The trends seen on Figs. 12 and 13 are similar for this element. The [Ni/Fe] value remains roughly at solar value until [Fe/H] ~ -0.3 dex. It has then a small decrease, almost step like and remains in a plateau until [Fe/H] reaches the solar value. From this point on it has two strong upturns at solar [Fe/H] and at $\sim +0.15$ dex. Between these values and from $\sim +0.15$ to the end of the metallicity range, we can observe the existence of two small plateau with solar [Ni/Fe] ratio and [Ni/Fe] $\sim +0.05$, respectively. Nickel abundances have a very low dispersion. We speculate that each one of these latter 'steps' might correspond to events that sparked an increase in the production of galactic Ni.

Our results are very similar to BEN, although a little different in their fine details: they only report one upturn at solar metallicity. We note a rough agreement with the results of CH00, SAD, FV05 and TAK as they all have or hint at the same general trends (slow decrease until solar value, then a weak upturn). Although BOD, GIL and GZ07 report similar trends, their results have an abundance slightly below ours in the whole [Fe/H] range (~ -0.05 dex). The same trends are also observed by AP04 but their abundance values are higher than most results and their slopes are also stronger.

6.5.5. Manganese

Contrary to all other elements, we observe an uniform increasing trend for [Mn/Fe] values from ~ -0.4 to 0.1 dex through the entire [Fe/H] range. In Figs. 12 and 13 we have the impression that two different branches exist for [Fe/H] values below ~ 0.1 dex. The manganese underabundance in this region seems to mirror the α elements overabundance.

There is a good agreement between our results and those of SAD and BOD. However, they do not find any hint of the existence of two separate branches. GIL and TAK results are different from ours: they show a plateau for [Fe/H] below the solar value.

6.6. The light metals: Mg, Na and Al

Sodium and aluminium are though to be mostly created in the core of massive stars (Chen et al. 2000), that later become SNe II. We can observe that the trends of Na and Al are similar to the alpha elements: we might even consider them mild alpha elements, even if we take into account the fact that they have an odd number of protons (McWilliam 1997). It is still difficult to differentiate the sources of Na and Al. Magnesium is theorised to be created only in SNe II supernovas, and can be considered a member of the alpha elements.

6.6.1. Magnesium

The [Mg/Fe] branches have a decreasing trend until [Fe/H] ~ -0.1, although the upper branch has a much steeper descent. Then, the branches join and the abundance remains constant at solar value. We can observe considerable scattering in the Mg plots. This is due to the fact that we

only used 2 or 3 lines per star in the determination of its abundance. Magnesium is a very interesting element: it is predicted that it can only be created in SNe II explosions (Chen et al. 2000), but we can see that there is not a continuous decline in magnesium as we would expect in this case (e.g. Chen et al. 2000; Bensby et al. 2003). Therefore, there must be a contribution of SNe Ia or other unknown factors that is causing the enrichment of Mg in the solar neighbourhood.

The obtained trends are similar to those of SAD, AP04, BEI, BEN, GIL and GZ07, but no author refers to a bifurcation below solar [Fe/H] value. CH00 have a similar trend but their plateau starts much earlier, at -0.3 dex, and the abundance value of this plateau in the whole range of [Fe/H] is higher than ours by 0.1 dex. TAK, on the other hand, have a systematic underabundance in the same plateau above solar metallicity when compared with our results.

6.6.2. Sodium

Sodium abundance values slowly decrease until they reach the solar value at [Fe/H] $\sim$ -0.2 dex. Then they remain constant in a metallicity region from [Fe/H] ~ -0.2 to ~ -0.1 dex. The abundance has an increasing trend for [Fe/H] $\gtrsim +0.2$. We suffer from considerable scatter in Fig. 12. It is easier to follow the trends in Fig. 13. There is also a slight hint in Fig. 13 that there might be a bifurcation below solar [Fe/H]. The trend of Na is similar to the alpha element trends, but the overabundance values at negative [Fe/H] are not so pronounced.

A similar behaviour was found by SAD as well as by BEI, FV05, GIL, BEN, TAK and GZ07. CH00 report a constant abundance value throughout the whole [Fe/H] range which is in disagreement with our results. No author mentions the existence of a plateau in the intermediate [Fe/H] region. No bifurcation is reported in any paper.

6.6.3. Aluminium

The aluminium trend is very similar to the alpha elements. One might say, at least from an observational point of view, that aluminium is an alpha element. Its abundance decreases until [Fe/H] $\sim$ -0.2 dex. Then it remains at constant abundance ($\sim +0.05$ dex) until [Fe/H] reaches +0.1 dex. Afterwards, there is an upturn followed by a plateau with [Al/H] $\sim +0.05$ in the [Fe/H] region between 0.2 and 0.4 dex. The trends are easier to see in Fig. 13, where we can also see the presence of a possible bifurcation similar to the one in the Mg plot. Again, we have even worse scattering than in sodium.

Our results are similar to those obtained by BEI, GIL, and BEN. CH00 and SAD have a different result from ours: the abundance remains constant at solar value and for CH00 it suffers an upswing toward higher metallicities when it reaches $\sim$ -0.3 dex.

7. Concluding remarks

In this paper we derived the abundances of 12 elements (Si, Ca, Sc, Ti, V, Cr, Mn, Co, Ni, Na, Mg, and Al) in a sample of 451 field dwarfs from the HARPS "high precision" GTO planet search program, from which **68** planets are known to harbour planetary companions. The spectroscopic parameters used in this study were derived by Sousa et al. (2008).

We compared our results with those presented in other works, in order to assure their consistency and reliability. The [X/H] distributions as well as the plots of the abundance ratios [X/Fe] vs [Fe/H] were analysed in order to compare the trends of stars with and without planets.

We also derived the galactic space velocity components and used them to kinematically select the origin of the stars of our sample, according to the method developed by Bensby et al. (2003, 2005). We found that the sample is comprised of 400 stars from the thin disk, 29 stars from the thick disk and 21 from a transition population that has characteristics from both populations. One star is from the halo.

We confirm that an overabundance for giant planet host stars is clear for all the studied elements. This may confirm previous suggestions that the efficiency of planetary formation correlates strongly with the metal content of the host star. In other words, the probability of finding a star with giant planets is greater in stars with high [X/H] ratios. The plot of the percentage of stars with planets as a function of the [X/H] ratio also gives us this information. This dependence is also predicted by recent studies of core-accretion modelling (see e.g. Ida & Lin 2004b, 2004b; Benz et al. 2006). We also confirm that stars hosting only neptunian-like planets may be easier to find around stars with similar or even lower metallicity than non-planet hosts. This suggests that lower mass planets may have a different kind of formation than that of jovian planets, which is also predicted by the aforementioned core-accretion studies of planetary formation.

We did not find any evidence of differences between stars with and without planets for the same [Fe/H] in the plots of [X/Fe] vs [Fe/H]. This is in general agreement with previous studies. The stars that harbour planetary companions simply seem to be in the high metallicity tail of the distribution, following the same trends as the stars without planets. This result favours the primordial origin as the preferred cause for the observed high metallicities in planet host stars.

We found a clear distinction between thick disk and thin disk populations when we analysed the [X/Fe] distributions, for [Fe/H] < 0. This extends to all elements except chromium and nickel, and confirms and extends the general results found by Fuhrmann et al. (1998) and Bensby et al. (2003, 2005).

Interestingly, however, we observe that in the plots of [X/Fe] vs [Fe/H] the populations of the thin and thick disk are mixed for the same [Fe/H] throughout the whole metallicity range. We do not see a clear separation be-

tween the populations as in Fuhrmann (2004) or Bensby et al. (2005). Instead, the plots of the alpha elements and Mg, for [Fe/H] < 0, reveal a bifurcation of two different groups of stars, both with stars from the three populations, that converge at [Fe/H] near the solar value. This bifurcation might also exist for V, Co, Na, and Al, but it is not clear due to scatter. In some of the plots (Si, Ca, Sc, Ti, Mg and Al) the two populations of this biffurcation seem to have different evolutionary dynamics: the one with lower abundances (dominated by thin disk stars) has a very soft slope (if any), while the higher abundance population (dominated by thick disk objects) has a much steeper slope, implying a more dynamic evolution.

In general, the trends that we found agree with the literature references, with the exception of the aforementioned bifurcation. Nevertheless, we note that the traditional separations between alpha elements, iron peak elements, and others might need to be reformulated as the elements tend to have differentiated trends, at least in the metallicity range of our study. Our results suggest that the origin of these elements is more complex than it is predicted by theory. Some elements show a considerable scatter (V, Co, Na, Al). We do not know if this scatter is cosmic or due to errors in the analysis.

Acknowledgements. V.N. acknowledges the support given by Fundação Calouste Gulbenkian (Portugal). N.C.S. would like to thank the support from Fundação para a Ciência e a Tecnologia, Portugal, through programme Ciência 2007 (C2007-CAUP-FCT/136/2006). We would like to thank the HARPS team for having provided us with the data for this paper.

References

Allende Prieto, C., Barklem, P. S., Lambert, D. L., & Cunha, K. 2004, A&A, 420, 183
Anders, E. & Grevesse, N. 1989, Geochimica et Cosmochimica Acta, 53, 197
Beirão, P., Santos, N. C., Israelian, G., & Mayor, M. 2005, ArXiv Astrophysics e-prints
Bensby, T., Feltzing, S., & Lundström, I. 2003, A&A, 410, 527
Bensby, T., Feltzing, S., Lundström, I., & Ilyin, I. 2005, A&A, 433, 185
Benz, W., Mordasini, C., Alibert, Y., & Naef, D. 2006, in Tenth Anniversary of 51 Peg-b: Status of and prospects for hot Jupiter studies, ed. L. Arnold, F. Bouchy, & C. Moutou, 24–34
Bodaghee, A., Santos, N. C., Israelian, G., & Mayor, M. 2003, A&A, 404, 715
Bond, J. C., Tinney, C. G., Butler, R. P., et al. 2006, MNRAS, 370, 163
Chen, Y. Q., Nissen, P. E., Zhao, G., Zhang, H. W., & Benoni, T. 2000, A&AS, 141, 491
Dehnen, W. & Binney, J. J. 1998, MNRAS, 298, 387
Ecuvillon, A., Israelian, G., Pont, F., Santos, N. C., & Mayor, M. 2007, A&A, 461, 171
Ecuvillon, A., Israelian, G., Santos, N. C., Mayor, M., & Gilli, G. 2006, A&A, 449, 809
ESA. 1997, The Hipparcos and Tycho Catalogues
Fischer, D. A. & Valenti, J. 2005, ApJ, 622, 1102
Fuhrmann, K. 2004, Astronomische Nachrichten, 325, 3
Fuhrmann, K., Pfeiffer, M. J., & Bernkopf, J. 1998, A&A, 336, 942
Gilli, G., Israelian, G., Ecuvillon, A., Santos, N. C., & Mayor, M. 2006, A&A, 449, 723
Gonzalez, G. 1997, MNRAS, 285, 403
Gonzalez, G. 1998, A&A, 334, 221
Gonzalez, G. & Laws, C. 2007, MNRAS, 378, 1141
Gonzalez, G., Laws, C., Tyagi, S., & Reddy, B. E. 2001, AJ, 121, 432
Haywood, M. 2008, A&A, 482, 673
Ida, S. & Lin, D. N. C. 2004a, ApJ, 604, 388
Ida, S. & Lin, D. N. C. 2004b, ApJ, 616, 567
Israelian, G., Santos, N. C., Mayor, M., & Rebolo, R. 2003, A&A, 405, 753
Johnson, D. R. H. & Soderblom, D. R. 1987, AJ, 93, 864
Kupka, F., Piskunov, N., Ryabchikova, T. A., Stempels, H. C., & Weiss, W. W. 1999, A&AS, 138, 119
Kurucz, R. 1993, ATLAS9 Stellar Atmosphere Programs and 2 km/s grid. Kurucz CD-ROM No. 13. Cambridge, Mass.: Smithsonian Astrophysical Observatory, 1993., 13
Kurucz, R. L., Furenlid, I., & Brault, J. T. L. 1984, Solar flux atlas from 296 to 1300 nm (National Solar Observatory Atlas, Sunspot, New Mexico: National Solar Observatory, 1984)
Laws, C., Gonzalez, G., Walker, K. M., et al. 2003, AJ, 125, 2664
Mayor, M., Udry, S., Lovis, C., et al. 2008, ArXiv e-prints
McWilliam, A. 1997, A&A, 35, 503
Piskunov, N. E., Kupka, F., Ryabchikova, T. A., Weiss, W. W., & Jeffery, C. S. 1995, A&AS, 112, 525
Robinson, S. E., Laughlin, G., Bodenheimer, P., & Fischer, D. 2006, ApJ, 643, 484
Sadakane, K., Ohkubo, M., Takeda, Y., et al. 2002, PASJ, 54, 911
Santos, N. C., Israelian, G., & Mayor, M. 2000, A&A, 363, 228
Santos, N. C., Israelian, G., & Mayor, M. 2001, A&A, 373, 1019
Santos, N. C., Israelian, G., & Mayor, M. 2004, A&A, 415, 1153
Santos, N. C., Israelian, G., Mayor, M., et al. 2005, A&A, 437, 1127
Santos, N. C., Israelian, G., Mayor, M., Rebolo, R., & Udry, S. 2003, A&A, 398, 363
Sneden, C. 1973, Ph.D. Thesis, Univ. of Texas
Sousa, S. G., Santos, N. C., Israelian, G., Mayor, M., & Monteiro, M. J. P. F. G. 2007, A&A, in press
Sousa, S. G., Santos, N. C., Mayor, M., et al. 2008, A&A, 487, 373
Takeda, Y. 2007, PASJ, 59, 335
Takeda, Y., Sato, B., Kambe, E., et al. 2001, PASJ, 53, 1211

Thielemann, F.-K., Argast, D., Brachwitz, F., et al. 2002, A&SS, 281, 25
Udry, S., Bonfils, X., Delfosse, X., et al. 2007, A&A, 469, L43
Udry, S., Mayor, M., Benz, W., et al. 2006, A&A, 447, 361
Udry, S., Mayor, M., Naef, D., et al. 2000, A&A, 356, 590
Valenti, J. A. & Fischer, D. A. 2005, VizieR Online Data Catalog, 215, 90141